LUND UNIVERSITY

Optimisation and Application of High-Order Harmonies of an ultra-Short Terawatt Laser

Hässler, Stefan; Swoboda, Marko

2004

[Link to publication](#)

Total number of authors:
2

Optimization and Application
of High-order Harmonics of an Ultrashort
Terawatt Laser

Report
by
Stefan Häßler and Marko Swoboda

Abstract

The process of High-Order Harmonic Generation is studied in Argon with ultra-intense femtosecond laserpulses, focusing on photon number optimization for the 19th harmonic order. First, a detailed description of the setup will be given before a one-dimensional model is introduced with the theory of the process to allow the interpretation of measurement data. Calculations of the model in *Mathematica* are performed and their results shown. Following is the presentation and interpretation of the measurement data. Finally, with the characterization of a fast VUV-diode a possible application of the harmonic radiation is presented.

Contents

Chapter 1

Introduction

Since its first realization in the 1960s the development of Lasers and their applications have had a tremendous impact on science as well as society. Lasers allow the generation of light with properties superior to that of most other radiative sources, be it in terms of coherence as well as intensity.
Intense and coherent light is also necessary for the effect under study in this work. It is provided by the Terawatt-Laser of the Lund Laser Centre, which ranks among the strongest of Europe's lasers.

1.1 High-Order Harmonic Generation

High-Order Harmonic Generation (HHG) is a nonlinear optical process when an incident strong laser field interacts with atoms, for instance in rare gases. Since the intensities needed for the process to occur are very high, only lasers with very short pulses obtained with the mode-locking technique led to the observation of the phenomenon in 1987. The introduction of *chirped pulse amplification* (CPA) methods in the early 1990's made table-top high-power laser systems available opening new possibilities to study this phenomenon.
When such an intense laser pulse is focused into the gas, odd harmonics of the laser radiation will be emitted. Their intensity will first decrease exponentially (or perturbatively), before a long plateau of equal-intensity-harmonics stretches to the so-called *cut-off region*, where an exponential decrease sets in again, until the harmonics have vanished completely.
An additional advantage of the high-order harmonic generation process is the preservation of the highly desirable properties of laser radiation for the extremely short wavelengths generated, such as narrow bandwidth, coherence (both spatial and temporal) as well as directionality and intensity.
These properties also yield possible applications of the generated harmonic radiation. The narrow bandwidth and small wavelengths suggest spectroscopic and imaging applications, for instance biologically and medically in the so-called water window. It has also been proposed to seed a free-electron laser in the x-ray spectral region.

1.2   Motivation Of The Present Work

High-order harmonics have been intensively studied in Lund, but the focus has not been on their optimization for quite some time now. Recent research focused mainly on attosecond pulses and their optimization. This left a setup for harmonic generation unused in some years, until one of the aims of our project was defined to be the reactivation of this setup. In addition, the investigation of the harmonic generation efficiency dependent on several parameters of the harmonic generator was also an aim to provide the ongoing research on attosecond pulses with ideas for the further optimization of the harmonic generation setup that is in use there. The optimized VUV light created with our own setup could be applied for measurements on ultra-fast photo-diodes.

Finally, this report should also provide a road map and manual for successive researchers on the same setup, allowing them to continue where we stopped.

Chapter 2

The Experimental Setup

This chapter gives an introduction to the laser system and a detailed description
of the harmonic-generator-setup in Lund. Based on this, other groups that are
to follow us shall be enabled to quickly get the setup going again and successfully
generate and study harmonics - i.e. as mentioned in section 1.2, this report shall
among others serve as a "harmonic cook book". That is why the description
will probably be unusually detailed.

2.1   The Terawatt Laser System In Lund

All work described in this report was carried out using the terawatt laser at the
Lund High-Power Laser Facility, which is part of the Lund Laser Center (LLC).
Since we were only users of the generated beam and did not work on the laser
system itself, this description will be rather brief.
The short pulses are generated using a Kerr-lens mode-locked Ti:sapphire oscil-
lator in which the dispersion is controlled by a set of prisms. The pump energy
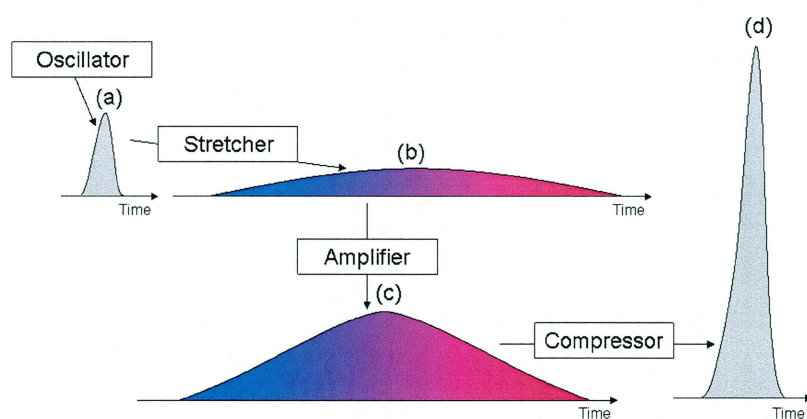is provided by an Ar-ion laser. Precise control over the temporal and spectral

Figure 2.1: Scheme of Chirped Pulse Amplification

characteristics of the laser pulses is achieved by means of an acousto-optical programmable dispersive light modulator - or Dazzler as it is commonly called. The obtained pulses are of $\approx$ 4 nJ energy and arrive with a frequency of 80 MHz.

To further amplify them, the system follows the chirped pulse amplification scheme (CPA, cf. Fig. 2.1), i.e. they are first stretched in time by a factor of $\approx$ 2500 using a grating-based stretcher that then introduces a positive chirp in the pulses. Some of the stretched pulses are now chosen by a pockels-cell (@ 10 Hz repetition rate) to enter a first amplification stage consisting of a cavity with another Ti:sapphire crystal as a gain medium that is pumped by frequency doubled Nd:YAG laser @ 10 Hz. A second amplification stage follows, where the pulses are sent into a 4-pass butterfly amplifier that again consists of a Ti:sapphire crystal that is pumped by two Nd:YAG lasers @ 10 Hz. Now the pulses have been amplified to typically 260 mJ energy.

They are finally compressed by two parallel gratings after having the beam diameter $(1/e^2)$ increased to 4 cm with a telescope to protect the compressors gratings. This compression is able to restore the original pulse duration but comes at the expense of losing pulse energy.

The final output are now pulses of $\approx$ 35 fs duration with $\approx$ 100mJ @10 Hz hence allowing peak powers up to 2 TW.

Since the launch of this system in Lund at 1992 with properties as described in [3] it has been continuously upgraded to achieve the pulse properties as described above. A major difference is an additional multi-terawatt arm that further amplifies the pulses up to 1.4 J energy and hence allows a peak power up to 40 TW. For the purpose of HHG this is of course an overkill and we were very well equipped with the output of the former described terawatt arm.

2.2   The Harmonic Generator In Lund

The principle setup for harmonic generation is outlined in Fig. 2.2. The laser pulses are -after being cut by an aperture- focused by a lens, whose position is adjustable over a range of $\approx$ 10 cm, into the vacuum chamber where they will pass the Ar gas medium, that is provided by different nozzles. The wavelength content of the beam is then split up by a grating and the harmonics can be detected by a Hamamatsu electron multiplier tube (EMT) whose signal voltage U is read by an oscilloscope. The oscilloscope's $U(\tau,\lambda)$ signal, where λ shall denote the wavelength chosen by the spectrometer and τ is the oscilloscope's time axis, is again read by a computer and integrated over a τ-region of interest. The computer also steers the grating position and thereby records a wavelength spectrum of the produced harmonic radiation.

We will now go through each part of the setup, including technical details that seem to be useful for future users of the Lund Harmonic Generator.

Beam

The light from the terawatt laser comes in a beam of $\approx$ 4 cm diameter. There are 3 irises in the beam path after the compressor that are carefully aligned once and then help to achieve proper alignment each day by adjusting the two mirrors, which guide the light to the harmonic generator, such that the beam,
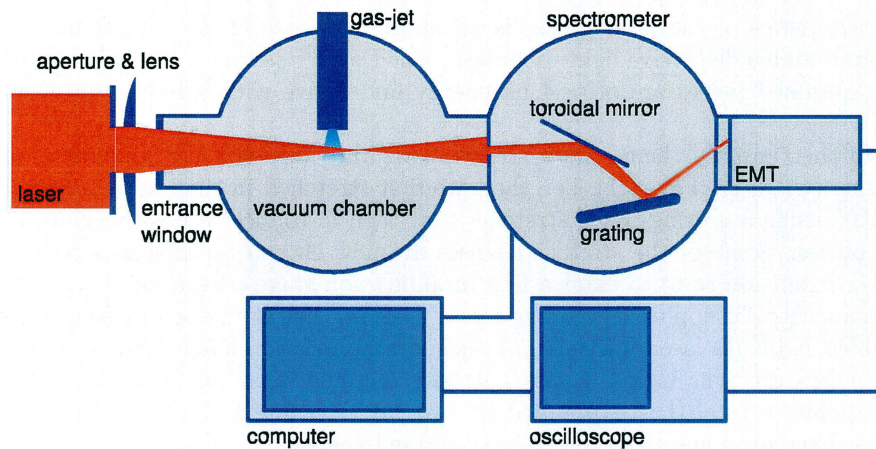
Figure 2.2: General setup of the Harmonic Generator in Lund

which has been cut by the first iris to get a sharply defined round spot, is sent through the remaining two irises and passes them properly.

The third iris is also used to adjust the beam radius z_i before focusing and hence the con-focal parameter b, which has great impact on the harmonic generation. The beam is then focused by a planoconvex lens of 1 m focal length. The convex side hereby faces the incoming beam to reduce aberrations and get a diffuse back reflection. The careful avoidance of any reflection of the incoming beam backwards and possibly into the laser system is always a serious issue. The lens can be moved along the beam propagation axis where an arbitrary scale is given by a ruler along which the lens holder is moved along. The beam waist is positioned under the gas valve at a lens position of ≈ 21 cm. It seems not useful to define this position as zero since the actual focus position can only be found with a precision of ± 1 cm which is due to the loose focusing geometry and the very rough method of observing the brightness of the plasma spark that is produced when the laser beam passes the Ar medium. Around this position the lens and hence the focus position with respect to the Ar medium can be moved ± 5 cm.

Vacuum Chamber

Preferably the whole beam path after the compressor should lead through vacuum since at high intensities like the ones achieved even without focusing, nonlinear effects in air like self-phase-modulation and the like can influence the pulses that finally reach the harmonic generator.

It seems however only essential to have the part of the path where the beam gets focused in vacuum. Furthermore the harmonic radiation has to be kept in vacuum of course, since its wavelengths extend to the VUV and even to soft x-rays which would be strongly absorbed in air. Also the EMT has to be kept in vacuum - in fact this is probably the spot in the setup, where the lowest pressure is necessary.

Vacuum is achieved by means of two turbo-molecular pumps of which one is positioned directly under the gas nozzle to efficiently pump away the supplied

Ar gas. The second pump is attached to the EMT to achieve the lowest possible pressure here. Two pressure meters -each actually consisting of two components to cover the desired pressure range- are position directly above the pump under the gas valve to be able to keep track of the pressure in the actual harmonic generation chamber and approximately in the middle between the two pumps to have a "worst pressure" estimate.

The pressure in the harmonic generation chamber reached down to $1 \cdot 10^{-6}$ mbar but reached about $\approx 2 \cdot 10^{-4}$ mbar when the gas supply was switched on.

Nozzles

Most of our measurements have been carried out with a very simple jet-nozzle before we built our own one to increase the medium length. Both are sketched in Fig. 2.3. The nozzle position can be adjusted by micrometer screws in 3 dimensions to properly hit the medium with the laser pulses.

The simple *jet-nozzle* provided a gas jet of approx. 2 mm width as could be estimated by moving the nozzle sideways hence scanning the jet across the beam and observe the signal of a certain harmonic. The signal drop was rapid when the jet was moved out of the beam so the 2 mm are fairly trustworthy. In several works [13] a gas jet produced by a nozzle like this one has been successfully described by a Lorentzian (that can be cut at the wings) atomic density profile. Our own nozzle was made with the goal to provide high Ar density over a longer distance hence being able to couple our large available laser energy into a large interaction volume which of course demands a quite good phase matching situation, i.e. a large coherence length. It should also be easy to build for several medium lengths. A "construction manual" is given in Fig. 2.6. We built two of them - one with a tube diameter of approx. 1 mm which we shall in the following call *thin-tube nozzle* and a second one with a larger tube of approx. 2.5 mm diameter that shall be named *fat-tube nozzle*.

The change of a nozzle takes some patience but is in principle easy to do. The critical point is, that the nozzle has to be pressed so tightly to the stamp (cf. Fig. 2.4), that the valve closes properly, but not too tight, such that valve wouldn't open any more. One can do this by applying some backing pressure and simply listening to the escaping gas or monitoring the decreasing backing pressure due to the leaking while screwing the nozzle in. Once the leaking stops, the valve is

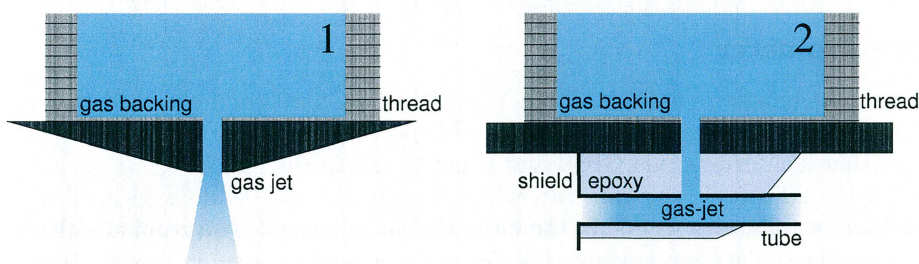Figure 2.3: (**1**) jet-nozzle, the gas is simply released through a hole on a tip and forms an ≈ 2 mm wide jet (**2**) tube-nozzle, the gas flows into a horizontal tube of variable length, the shield protects the epoxy from the beam during the alignment

very sensitive to further movement. The right position is found within a very narrow angle interval.

Gas Supply

Throughout the present work we used Ar gas as a medium. The gas is supplied by a pulsed piezoelectric valve, whose functioning is sketched in Fig. 2.4. The valve is pulsed to have sufficiently high Ar pressure when the laser pulse arrives and on the other hand avoid increasing the background pressure in the chamber. The triggering was done by a valve driver, that directly puts a voltage on the piezoelectric crystal that opens the valve. This driver was again triggered by a delay generator that got its input directly from the terawatt laser's trigger signal. Such it was possible to precisely control the opening time of the gas valve with respect to the incoming laser pulses. We chose a timing such that the valve closes 3 μs after the pulse has passed and opens 1 ms before that. Opening for 1 ms at the laser trigger's frequency of 10 Hz means that the valve remains closed 99% of the time.

The backing pressure, which denotes the Ar pressure that drives the gas out of the valve (cf. Fig. 2.4), can be set by a control device that simply monitors the pressure in the reservoir and refills it automatically to maintain the set value.
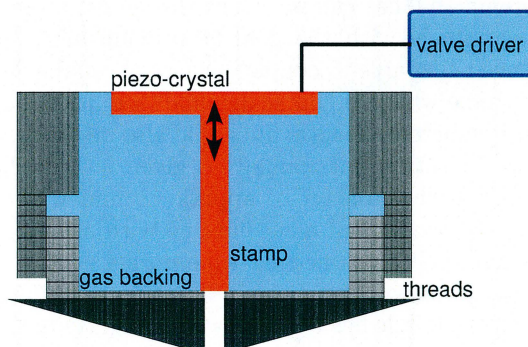
Figure 2.4: Functioning of the piezoelectric valve. A piezo-crystal lifts up the stamp hence opens the valve.

Spectrometer

The spectrometer is a I.S.A. Jobin-Yvon PGM PGS 200 and sketched in Fig. 2.2. Between the computer an the actual spectrometer there is still a control unit that is addressed via GPIB and is not drawn in the figure.

After the adjustable entrance slit, which enables the user to do a spectral resolution vs. intensity trade-off, the entrance slit is imaged by a toroidal mirror on the plane platinum grating. Its 450 grooves per mm give an optimal spectral range of 16 - 80 nm. The fundamental wavelength is then cut away by a fixed screen to protect the EMT from its high intensity and only the desired harmonic wavelengths pass to the exit slit which again is changeable. For the configuration of a 200 μm entrance slit and a 100 μm exit slit the resolution is given as 0.5 nm for the range of 52 to 60 nm.

Using an entrance slit means in particular, that we do not image the focus of the laser beam hence the harmonic near fields onto the grating but the fields as they are at the slit. We look at the far field, which allows us to see spatial properties of the harmonic beam.

We used an 100 μm exit slit and in most cases adjusted the entrance slit to 100 μm as well.

Detection And Data Acquisition

The principle setup is shown in Fig. 2.5. The oscilloscope is triggered by a diode that looks at the back reflection of the laser beam at the last iris. It records an U(τ,λ) signal from the EMT, to which a voltage of 4000 V is applied and which should be aligned, too. "Aligned" means in this case, that it should have a support and one should try to find a position where the signal of a harmonic (provided that the spectrometer is set to a corresponding position) is maximal. This can enhance the signal significantly! There is a pre-amplifier between oscilloscope and EMT to protect the sensitive oscilloscope channels.

The computer program records this U(τ,λ) curve at times given by the laser trigger (that is shared with the gas supply's delay box and put into the computer's parallel port) hence copies one curve per incident pulse via GPIB. It then integrates this voltage curve over a τ-region of interest which is chosen by the oscilloscope's cursors and read by the computer program. This integral is the value that is plotted vs. the wavelength as chosen with the spectrometer and is proportional to the photon number at this spectral position.

The program is also capable of evaluating the diode signal and eliminate signal variations due to energy fluctuations in the incident pulses but that wasn't necessary for our purpose.
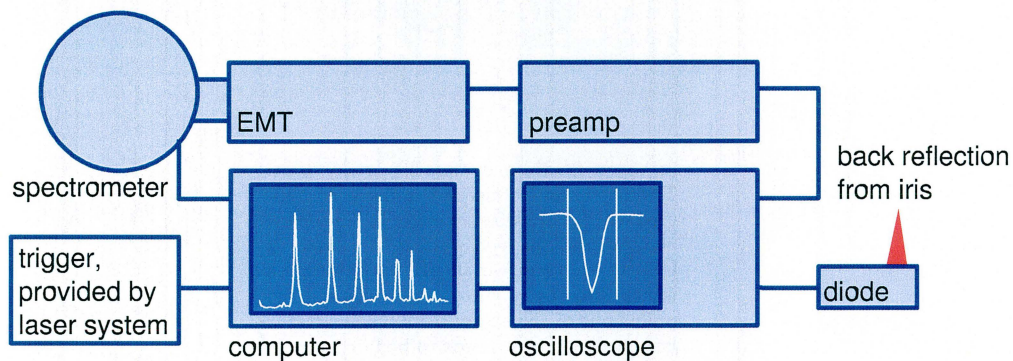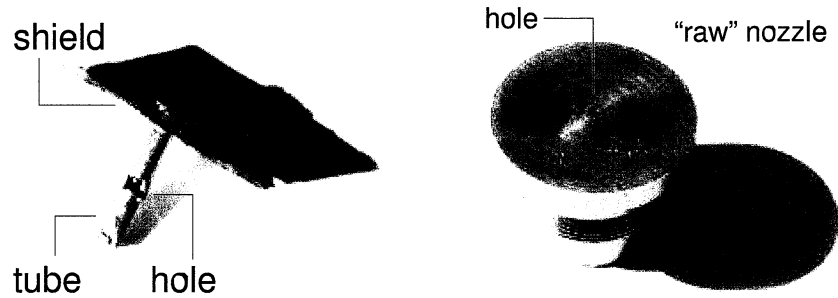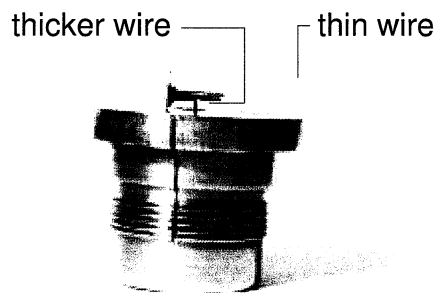

Figure 2.5: The components to record a wavelength spectrum.

(a) *Step 1:* Cut a canule of 1 mm diameter to the desired length. Cut a small hole in with a hacksaw. Cut a shield from some ≈ 0.5 mm thick Al foil, prick in a hole that fits the tube.

(b) This is the simplest nozzle possible as it is available in the accessories of the gas supply. We will use one like this.

(c) *Step 2:* Here comes the tricky part: The tube can be cleaned and easier handled with a thin wire through it. The channel through the epoxy from the nozzle's hole to the one we sawed into the tube is kept free by a wire. This wire will be pulled out of the epoxy from below after it has hardened so it needs to be fairly stable hence not too thin. For this purpose one has to find a wire whose diameter fits our needs (e.g. copper wire of 0.5 mm diameter works fine) and get it to stick just a bit out of the nozzle. On this tip we now balance our tube such that the wire sticks into the tube's hole. Together with the shield this should now give the tube a horizontal position which is of course crucial to be able to align our construction properly to the laser beam later on. Now put epoxy around such that the tube is fixed to the nozzle and the gas channel can be formed. After letting it harden sufficiently long pull out both wires. If everything went fine, the tube-nozzle should be finished and ready to be built in.

Figure 2.6: How to build a tube nozzle for a desired medium length

Chapter 3

Theoretical Description

In this chapter some physical and theoretical foundations of the harmonic generation process will be discussed and described. The first section will deal with effects occurring at the optical field strengths required for harmonic generation and their implications for the experiment. The second section will deal with focused laser beams and their description as Gaussian beams. Finally, a third section will describe high-order harmonic generation and its aspects.

3.1 Atoms in Strong Fields

Focusing intense and short laser pulses will result in very high intensities in the focus and thus very high fields. Their order of magnitude exceeds the regime of conventional linear and nonlinear optics. The medium can no longer be seen as negligibly ionized, since ionization probabilities will increase with field and intensity.

Ionization is not only non-negligible but even provides the dominating contribution in this strong-field-regime to the medium's polarization since the oscillating motion of the electrons that managed to leave their atoms is of much larger amplitude than an atomic radius and the created ion's polarizibility is significantly smaller than the one of a neutral atom. Thus the treatment of the induced polarization cannot be perturbatively any more, i.e. considering electrons in their lowest bound state which gets slightly perturbed by an incident field, but the ionization process and subsequent movement of the electron in the continuum are to be considered.

Ionization Processes

There are three different types of ionization processes that occur with strong fields and high intensities. They are depicted in figure 3.1.

Multiphoton Ionization

In multiphoton ionization several photons interact with an atom at the same time, providing the necessary energy to overcome the binding energy $-W_B$ and releasing the electron to the continuum. The probability for the process to occur is dependent on the number N of photons required to ionize the atom. This
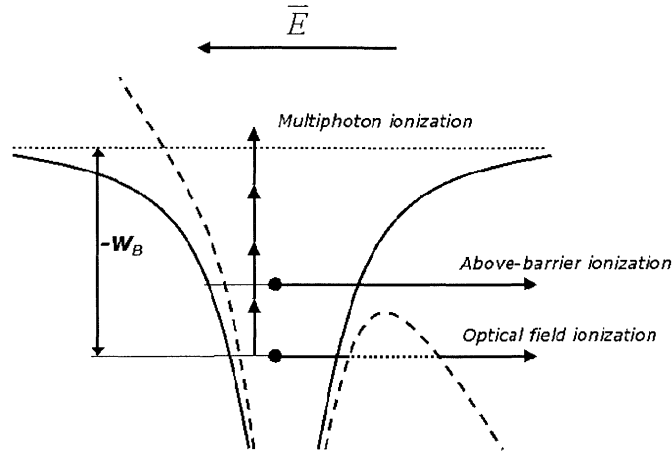
Figure 3.1: Regimes of atomic strong field ionization. The dashed line resembles the strongly perturbed atomic potential due to high optical field strength. The higher state depicted with Above-barrier ionization is not an excited state inside the atom but is supposed to represent the ground state in an even stronger bent atomic potential.

leads to a proportionality of $P \sim I^N$.
This type of ionization is always present but plays a rather negligible role with the intensities being dealt with in our experiment.

Optical Field Ionization

If the laser field approaches the strength of the atomic field itself, the atom's Coulomb potential will be so strongly suppressed that the wave function of the valence electron will be able to penetrate the barrier that separates it from the continuum via a tunneling process. This will give rise to a form of ionization called *optical field ionization*. In fact, the probability will be several orders of magnitude higher than that of multiphoton ionization.
The probability of optical field ionization is dependent on laser frequency and barrier width, thus intensity. The stronger the field, the narrower the barrier at top field strength and thus the higher the tunneling probability. Still, the laser frequency determines how much time will be given to the electron to consider the tunneling process. Thus, if the frequency is too high, i.e. exceeding that of near-infrared radiation, the potential will alternate too quickly and the electron will not tunnel out of the atom with a considerable probability. This results in the ionization regime dominance going directly from Multiphoton ionization to Above-barrier ionization.

Above-Barrier Ionization

In this regime of atomic ionization, the laser field suppresses the atom's Coulomb-potential so strongly, that no tunneling process is required anymore for ionization.

Refractive Index

The presence of free electrons influences the refractive index by the oscillation of these electrons with the optical field. Their oscillation is described by the plasma frequency

$$\omega_P = \sqrt{\frac{e^2 n_e}{m \varepsilon_0}} \tag{3.1}$$

where e is the electron charge, m the electron mass, ε_0 the vacuum dielectric constant and n_e denotes the electron density. The refractive index is then given by

$$n = \sqrt{1 - \frac{\omega_p^2}{\omega^2}} \tag{3.2}$$

with ω as the incident laser frequency.

The electron density is greatly dependent on the local field strength (due to its importance for the ionization probability), whose distribution is given by the laser intensity distribution. Since it is sufficient for the considerations here to assume a coaxial Gaussian intensity profile and our laser pulses are very short so the electrons will not move significant distances, this will result in the same distribution of free electrons. These will shape a diverging lens in accordance with equation 3.2 leading to an actual defocusing of the laser beam in the focus. H.T. Kim et al. [10] studied this intensively with the aim of coupling a large laser pulse energy into a large interaction volume and not only obtained a defocusing but even a self-guiding of the beam. This may occur, when the defocusing compensates the converging laser beam. If the ionizing medium is placed before the laser focus, the central part of the fundamental beam will be refracted outwards due to higer electron concentration at the centre, whereas the less-affected outer parts are still converging. This forms a flattened radial profile which in turn leads to a flattened electron density profile that changes rapidly at the boundary of the beam. The formed refractive index profile will hence exhibit a a sharp increase at the boundary constituting a waveguide for the laser beam. This can significantly enhance the effective harmonic generation volume and thereby the conversion efficiency.

Another interesting effect occurs for furtherly increasing intensities, when the electron mass increase due to their acceleration to relativistic speed becomes no longer negligible. Then the effect will reverse giving rise to relativistic self focusing, since then the highest mass is connected to the highest intensity and thus again a focusing lens is shaped. In equation 3.1 the influence of electron mass m on the plasma frequency can be seen. Since the intensities of our experiment seldom reached the threshold for this effect to occur, self-defocusing is assumed to dominate under our conditions.

3.2   Gaussian Beams

A very commonly used and easily handled E-field solution that can be used for the description of laser beams is that of the Gaussian beams. It can be derived from the paraxial wave equation or the Fresnel-Kirchhoff integral, which shall not be considered here.[5]

In a Gaussian beam the optical field decreases from its maximum at the center with the perpendicular coordinates like a Gaussian function. It is radially symmetric and starts with a beam waist with diameter w_0. At the waist the equiphase surface radius is infinite and z is usually set to be zero.

Figure 3.2 schematically shows a Gaussian beam with waist and equiphase fronts.
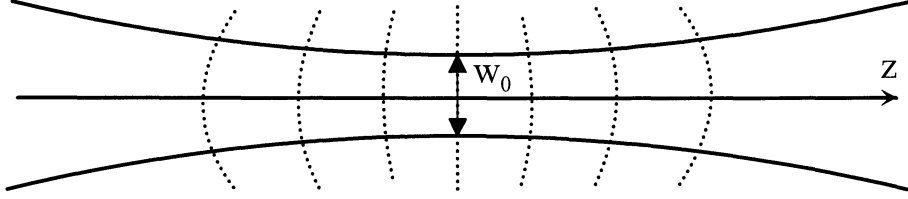

Figure 3.2: Profile of a Gaussian beam, continuous curves, and equiphase surfaces, dashed curves

Propagation

The E-field distribution of a Gaussian beam is completely described by a beam waist diameter w_0, the propagation coordinate z and the wavelength λ. R is the radius of an equiphase surface of the extending wave and k is the wave vector. The expression for the field amplitude is

$$u(x, y, z) = \frac{w_0}{w} \exp\left[-\left(\frac{x^2 + y^2}{w^2}\right)\right] \exp\left[-ik\left(\frac{x^2 + y^2}{2R}\right)\right] \exp i\phi \qquad (3.3)$$

with

$$\phi = \arctan\left(\frac{\lambda z}{\pi w_0^2}\right) \qquad (3.4)$$

At $z = 0$ the intensity distribution is known, since $w_0 = w$ - it follows a Gaussian function.

For expressing the beam properties, we define the *Rayleigh range*

$$z_R = \frac{\pi w_0^2}{\lambda} \qquad (3.5)$$

which allows us to express the spot size as

$$w^2(z) = w_0^2\left[1 + \left(\frac{z}{z_R}\right)^2\right] \qquad (3.6)$$

the spherical wavefront radius as

$$R(z) = z\left[1 + \left(\frac{z_R}{z}\right)^2\right] \qquad (3.7)$$

and the longitudinal phase as

$$\phi(z) = \arctan\left(\frac{z}{z_R}\right) \qquad (3.8)$$

As can be seen in Figure 3.2 there is a phase jump of 180 degrees at the beam waist, also called the *Gouy phase shift*. This will be referred to later.

If now a Gaussian beam is transformed by an optical system, it is most conveniently described by the system's *ABCD matrix*. This matrix consists of four elements and couples the complex beam parameter q of the beam before and after the system. The parameter q can be viewed as the curvature of a spherical wave, but complex. With separated real and imaginary part it can be written as

$$\frac{1}{q} = \frac{1}{R} - i\left(\frac{\lambda}{\pi w^2}\right) \tag{3.9}$$

and its transformation by an optical system with the matrix

$$S = \begin{pmatrix} A & B \\ C & D \end{pmatrix}$$

is described by

$$\frac{1}{q_2} = \frac{C + (D/q_1)}{A + (B/q_1)} \tag{3.10}$$

Truncated Gaussian Beam

Since in our experiment the beam was cut by an aperture before the lens, we did not deal with perfect Gaussian beams but cut ones, so-called *truncated Gaussian beams* [1]. The beam will first pass an aperture with a radius a and then be focused by a lens with focal length f. So right after the lens ($z = z_0$) the field distribution is given with the field amplitude $\tilde{E}_0$

$$E_0 = \tilde{E}_0 e^{-r_0^2/w(z_0)^2} e^{ikr_0^2/2f} \quad r_0 \leq a \tag{3.11}$$
$$E_0 = 0 \quad r_0 > a$$

The phase factor describes the phase acquired by the beam passing through the lens. Truncated Gaussian beams' intensity changes slower around the focus but the phase varies faster. This might affect phase-matching.

3.3 High-Order Harmonic Generation

Electron Motion

The classical description of the electron's motion is in fact quite an accurate way to calculate the further evolution of the free electron wavepacket, that has been created in an ionization process. To be precise, the wavepacket's center of mass will be under observation here, proving itself sufficient to most of our needs. It was shown that the wavepacket extends typically at a rate of less than $1\,nm/fs$ due to quantum diffusion and hence during a laser period remains small compared to the amplitude of its oscillation in the laser field which is $\sim 10\,nm$ (Delone and Krainov, 1991).

Assuming the laser field to be linearly polarised and neglecting any field from the source ion the equation of motion for our electron is

$$m\ddot{x} = -eE_a e^{-i\omega t} + c.c. \tag{3.12}$$

which has a solution of

$$\tilde{x}(t) = a_w e^{-i\omega t} + c.c. \tag{3.13}$$

where the jiggle amplitude is

$$a_w = \frac{eE_a}{m\omega^2}. \tag{3.14}$$

The time-averaged kinetic energy of this motion is readily accessible by $K = \frac{1}{2}m\left\langle \dot{\tilde{x}}(t)^2 \right\rangle$ which with

$$\dot{\tilde{x}}(t)^2 = (-i\omega x)e^{-i\omega t} + c.c.$$

gives

$$K = \frac{e^2|E|_a^2}{4m\omega^2} \tag{3.15}$$

which is referred to as *the ponderomotive energy* of the electron in the laser field.

The movement of the free electron (eq. 3.13) is linear with the field amplitude. However, we are not dealing with a free electron gas of constant density here, but with an ionizing medium. Electrons might move in close proximity to atoms respectively ions and furthermore the strong field $\tilde{E}$ not only causes some electrons to oscillate but also creates new electrons by means of optical-field-ionization for which the rate is strongly field-dependent. This will certainly introduce nonlinearities.

The Semiclassical Model

There is an easy way to understand High-Order Harmonic Generation and the occuring plateau on a semiclassical level, giving an intuitive understanding of the phenomenon.

1. The laser intensity is sufficiently high to initiate optical-field-ionisation as described above.

2. The electric field accelerates the free electron away from the ion. When the electric field changes sign, the electron is accelerated back to and has the possibility to return in the vicinity of the ion again. The probability for this to occur is of course only significant for linearly polarised laser light.

3. When to electron is close to the ion, there's a certain probability for re-combination back to the ground state. The captured electron emits all its captured kinetic energy plus the ground state binding energy I_p as a photon.

This process will occur twice in each laser period. The emitted train of light pulses in the time domain corresponds to a discrete frequency spectrum. The period in time was half a laser period hence the frequency period is $2\omega_0$.

A closer look reveals, that the energy gained and hence emitted by the electrons, depends on the phase of the electric field at the time of emission and recombination. This may sound more complicated than it is - for each tunneling-time,
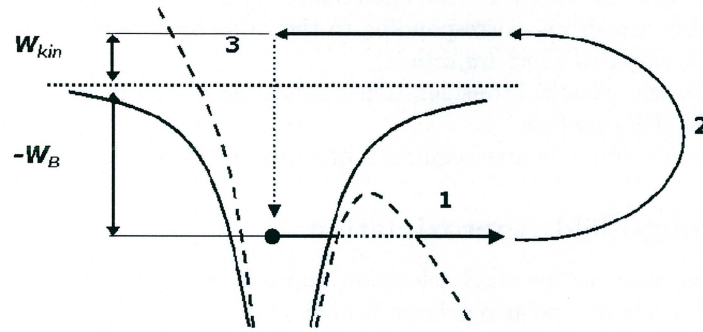
Figure 3.3: Semiclassical Three-Step Model for High-Order Harmonic Generation. (1) The electron leaves the atom by optical field ionization, then (2) is accelerated in the external field, first away from the ion but then back with the switching field, gaining kinetic energy, where it (3) recombines with the ion-core, emitting radiation.

it is easy to calculate the electron's trajectory and hence find the time when the electron meets the ion-core again and the kinetic energy that it has at that time (*with just the same classical eq. of motion (3.12) as above and the initial condition that $x(t_t) = 0$, where t_t is the tunneling time.*) This leads to the plots shown in fig.3.4.

   First of all - there are only certain tunneling times, for which the corresponding trajectories lead back to the ion core. Those are the interval from the field peak until the zero crossing of teh field amplitude. Among these, the possible return energies are distributed between zero and a maximum, that turns out to be $\approx 3.2K$. The cutoff position of the created harmonics can therefore be predicted to be

$$q_{max}\hbar\omega_0 = I_p + 3.2K. \tag{3.16}$$

Furthermore, we see, that the emitted photon can have any energy between I_p and $I_p + 3.2K$. Why there is a discrete spectrum of odd harmonics instead of white light can again be explained as above by the $T/2$ periodicity of the generating process.
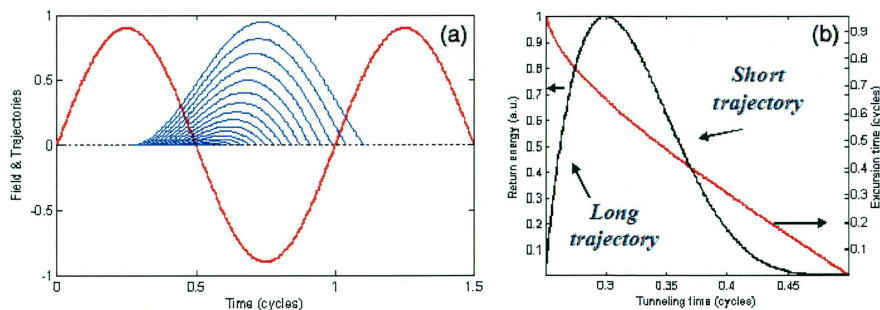

Figure 3.4: (a) Electric field and trajectories for different tunneling times of the electron. (b) Return energies and corresponding excursion times. [8]

Second, one obtains -except for the maximum- two possible trajectories for each return energy, which we -corresponding to their different excursion time- shall denote with *long* and *short trajectory*.
This simple, semi-classical consideration shows already a large part of the properties of the HHG process.
The full description of course requires a quantum mechanical treatment.

The Strong-Field Approximation

Consider an atom in the single electrion approximation, that was mentioned above and a linearly polarized laser field $\mathbf{E}(t) = (E(t)\cos(\omega t), 0, 0)$. In the length gauge, the Schrödinger equation then writes as

$$i\hbar|\Psi(x,t)\rangle = \left[-\frac{\hbar^2\nabla^2}{2m} + V(x) - E(t)\cos(\omega t)ex\right]|\Psi(x,t)\rangle, \qquad (3.17)$$

where $V(x)$ is the atomic potential. Initially, the atom shall be in the ground state, denoted as $|0\rangle$.
It is further assumed that all conditions are such that the regime of optical-field-ionization, i.e. the tunneling regime is valid. The intensities are large enough, so that intermediate resonances, i.e. other bound states than $|0\rangle$, including dynamically induced ones (by the large shift of states due to the strong incident field), play no role. Still, the intensities shall be below the saturation level, when all atoms ionize during the laser pulse.
The electron undergoes transitions to continuum states, that shall be labelled by their kinetic momentum at the time of release $|q\rangle$, which are eigenstates of the free Hamiltonian, i.e. the Hamiltonian without the incident laser field,

$$\left[-\frac{\hbar^2\nabla^2}{2m} + V(x)\right]|q\rangle = \frac{q^2}{2m}|q\rangle.$$

Actually the contribution of the atomic potential $V(x)$ is very small since typically the electron will tunnel out at a very high laser field value and the force $-\nabla V(x)$ becomes negligible. Subsequently, the electron gets accelerated and quickly acquires a high velocity, so the role of $V(x)$ is really small. At the turning points of the electron's jiggle-motion, its velocity will of course be small but these points are typically very far from the nucleus *(note that the jiggle-amplitude a_w was much larger than the atomic radius would typically be)*. So $V(x)$ can as well be omitted here.
The above considerations suggest the following assumptions, that characterize the Strong-Field-Approximation:

1. All bound states of the atom are neglected except the ground state $|0\rangle$.

2. In the continuum, the electron can be treated as a free particle moving in the electric field of the laser.

3. The depletion of the ground state is neglected.

Obviously, assumption 2 holds only for electrons with high velocities in the vicinity of the ion core and hence those that are responsible for the generation

of high harmonics: $q\omega_0 > I_p$. It is included in the calculation by the continuum-continuum matrix-element

$$\langle q|ex|q'\rangle = ie\hbar\nabla_q\delta(q - q').$$

Assumption 1 implies, that the electron wave function can be expanded as

$$\psi(x,t)\rangle = e^{iI_p t/\hbar}a(t)|0\rangle + \int d^3q \, b(q,t)|q\rangle,$$

where $a(t)$ is the ground state amplitude, which, according to assumption 3 is set unity, and $b(q,t)$ are the amplitudes of the continuum states.
The following calculation is carried out in the space spanned by $|0\rangle$ and the continuum states $|q\rangle$, i.e. the Hamiltonian governing the evolution of $\Psi(x,t)$ is projected onto this space yielding a Schrödinger equation for the continuum amplitudes $b(q,t)$ which can be solved analytically.
The solution is

$$b_0(q,t) = i\int_0^t dt' \, E(t') \cos(\omega t')d_x(p - eA(t')/c) \, e^{-iS(p,t,t')/\hbar}. \tag{3.18}$$

The b's index 0 indicates, that the obtained amplitudes are a zeroth order solution, i.e. calculated by completely omitting the atomic potential. It is also possible to include rescattering of the electrons by treating $V(x)$ as a small perturbation.
$d_x = \langle q|ex|0\rangle$ is the atomic dipole matrix element. The canonical momentum $p = q + eA(t)/c$ was introduced, where $A(t)$ is the laser field's vector potential. $S(p,t,t')$ is the quasi-classical (because of the classical vector potential A) action,

$$S(p,t,t') = \int_t^{t'} dt'' \left(\frac{(p - eA(t'')/c)^2}{2m} + I_p\right)$$

Eq.3.18 is to be interpreted as a sum of probability amplitudes that the electron is born in the continuum at the time t' with the canonical momentum p. These two amplitudes are then propagated until time t, aquiring a phase factor $\exp[-iS(p,t,t')/\hbar]$.
With these b_0s it is possible to calculate the electronic wave function and hence the induced time-dependent dipole moment.
After some more work (in the framework of Feynman's path integrals) it turns out, that for the qth Fourier component of the dipole moment (corresponding to the qth harmonic) can be written as a sum over all relevant trajectories (quantum paths) that are selected by being stationary values of the quasi-classical action S (in analogy to the classical Lagrange principle $\delta S = 0$),

$$ex_k = \sum_n a_n \exp[-i\alpha_n I]$$

where a_n is an amplitude and α_n is a proportionality factor between the incident intensity I and the aquired dipole phase, which are characteristic to each trajectory.

α_n is a factor found when plotting the dipole phase $\phi_{d,n} = S(p_n, t_n, t'_n)/\hbar$ vs. the incident intensity for a certain harmonic q. At intensities for which this q^{th} harmonic is part of the plateau, the dependence is found to be linear with slope α_n.

Fig. 3.5 shows the quantum path contributions to the dipole phase of the 35th harmonic. Clearly, above the cutoff intensity for this harmonic one finds two dominating paths - nicely corresponding to the two trajectories, that were found in the classical consideration. The obtained $\alpha_{\text{SP}} \approx 1 \cdot 10^{-14}\, cm^2/W$ for the short path and $\alpha_{\text{LP}} \approx 24 \cdot 10^{-14}\, cm^2/W$ for the long path vary only slightly with the harmonic order.

Plotting the dipole strength, i.e. the absolute value of the obtained dipole moment, for a certain harmonic q vs. the incident intensity one finds a I^β power-dependency for the intensity region, where the qth harmonic is part of the plateau.

Hence we can use a single-atom dipole moment consisting of Fourier components of the form

$$d_q \propto I^\beta \left(e^{-i\alpha_{\text{SP}}I} + e^{-i\alpha_{\text{LP}}I} \right) \tag{3.19}$$

with the two α_i given above and a β that is dependent on the medium and the harmonic order.

The qth Fourier component of the induced polarisation in the generating medium will simply be

$$P_q(\mathbf{r}) = N_a(\mathbf{r})d_q, \tag{3.20}$$

where $N_a(\mathbf{r})$ is the atomic density at position $\mathbf{r}$ in the medium.
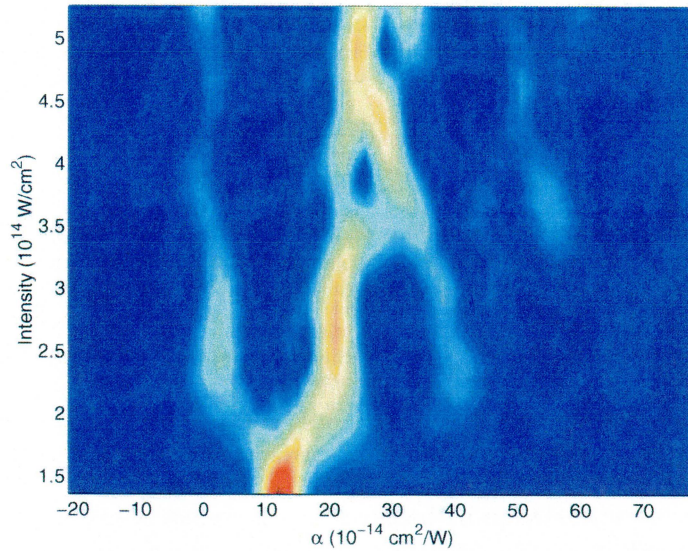

Figure 3.5: Quantum path contributions to the dipole phase of the 35th harmonic at different laser-intensities. α is the slope of the intensity dependence of the contribution. Yellow-red corresponds to high contribution and green-blue to low contribution. [1]

Phase Matching

For nonlinear processes like sum-frequency generation, where the interaction and superposition of several light waves is required phase matching considerations play an important role for the conversion efficiency. It also is important in high harmonic generation.

Essentially, the difference of the wavevectors $\vec{k}$ of the generated harmonic beam and the incident laser beams has to be minimized to allow the most efficient energy transfer between them. We will first look at second-harmonic generation in the perturbative approximation. We write

$$E_1(z,t) = \frac{1}{2}\left[E_1(z)e^{i(k_1 z - \omega_0 t)} + c.c.\right] \tag{3.21}$$

for the incoming field that propagates in z-direction and

$$P_2^{NL} = \varepsilon_0 \chi^{(2)} E_1^2 = \varepsilon_0 \chi^{(2)}\left[E_1^2(z)e^{i(2k_1 z - 2\omega_0 t)} + c.c.\right] \tag{3.22}$$

for the nonlinear polarization, that results in a harmonic wave

$$E_2(z,t) = \frac{1}{2}\left[E_2(z)e^{i(k_2 z - 2\omega_0 t)} + c.c.\right] \tag{3.23}$$

with the double frequency. So if we now compare $2k_1$ with k_2 we will find that if $2k_1 \neq k_2$ the polarization and the generated harmonic field will propagate at different phase velocities, thus will get out of phase with each other. We introduce the phase mismatch $\Delta k = k_2 - 2k_1$ that has to be minimized.

This finite wave vector mismatch can for example result from different refractive indices for different wavelengths in dispersive media.

Figure 3.6 schematically shows the effects of phase mismatch. The second-order polarization builds up $2\omega_0$ wavelets at different positions of the medium, which are out of phase. Therefore they will propagate differently and only build up constructively for a certain propagation length L_{coh} in the medium. Over this distance the polarization and the $2\omega_0$-wave get dephased by π, so that

$$L_{coh} = \frac{\pi}{\Delta k}$$

So the most ideal condition is achieved when $\Delta k = k_2 - 2k_1 = 0$, corresponding to perfect phase matching, when no dephasing occurs at all and thus the intensity of the generated wave builds up continously during the propagation in the medium.

On-Axis Phase Matching

In our present case of high-order harmonic generation several other phase effects have to be taken into account.

We define a phase mismatch depending on the harmonic order as

$$\Delta k = k_q - qk_1 \tag{3.24}$$

The phase of a Gaussian beam is

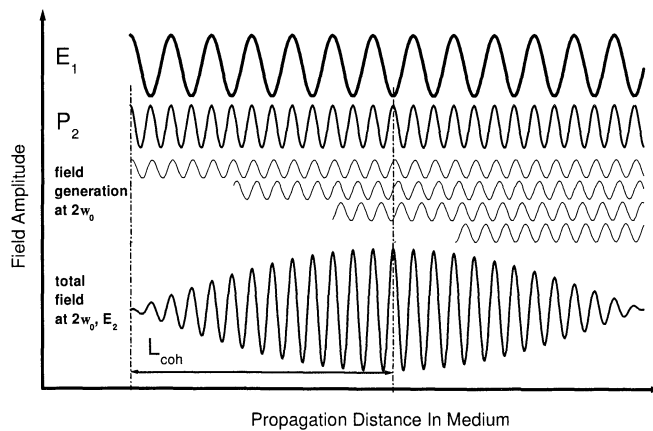$$\phi_G = k_1 z - \arctan\left(\frac{z}{z_R}\right) \tag{3.25}$$

Figure 3.6: Illustration of the effect of phase mismatch. On the top the laser field is shown, below that the induced 2nd order polarization. Below different wavecomponents at the higher frequency are generated at different positions of the medium. At the bottom the resultant field of the second harmonic is shown, which will decrease again after a propagation distance L_{coh} due to the mismatch. [1]

In addition to that we have to take into account the intensity-dependent phase of the single atom's dipole moment

$$\phi_{dip} = -\alpha_i I(z) \qquad (3.26)$$

where α_{SP} corresponds to the short and α_{LP} to the long trajectory of the HHG process, that have to be considered separetely.

A phase mismatch resulting from the free electrons created at these high intensities also has to be treated. As we saw in section 3.1 the refractive index of the gaseous medium is dependent on the oscillation of the free electrons at the plasma frequency ω_p and the light frequency itself, leading - for high-order harmonics - to

$$n_q^e = \sqrt{1 - \frac{\omega_p^2}{q^2 \omega_0^2}} \qquad (3.27)$$

with q as the harmonic order. This leads to a free-electron wave vector mismatch

$$\Delta k_q^e = k_q^e - q k_q^e = -\frac{\omega_p^2}{2 c q \omega_0}(q^2 - 1) \qquad (3.28)$$

which dominates over the dispersion of the medium already at relatively weak ionization.

3.4 A Simple 1D Model

In order to interpret our experimental results and develop ideas for the optimization of the harmonics, we will now introduce a simple 1-dimensional model

for the HHG process. It uses the single atom dipole moment as given by eq. 3.19 that had been derived applying the Strong Field Approximation and propagates this polarisation through the generating medium.

The local dipole moments at the qth harmonic frequency will of course take the phase of the incident laser field ϕ_L. Hence we can write

$$f_q = e^{iq\phi_L(z)} I^\beta \left(e^{-i\alpha_{\text{SP}} I} + e^{-i\alpha_{\text{LP}} I} \right) \quad \propto d_q \qquad (3.29)$$

where q is the considered harmonic order and f_q can just be considered as a "single atom answer" to the incident field that is proportional to the actual dipole moment.

We assume $\beta = 3$ for our model. Other authors that dealt with argon didn't publish the β they used but just that it was smaller than the harmonic order. So this choice was taken from an empirical formula [9] that is valid for Ne but proved to give reasonable results for us as well. One could introduce a Heaviside function before the I^β to take the threshold intensity for the generation of the qth harmonic as given by eq. 3.16 into account. We simply note that this threshold is $\approx 7 \cdot 10^{13} \, W/cm^2$ for q=19 in argon. This threshold is reached (for the three iris diameters considered) at approx. ± 2 cm distance from the beam waist.

We will omit the long trajectory from here on for simplicity as well as to speed up calculations. The dipole phase of this long trajectory has a much steeper intensity dependence ($\alpha_{\text{LP}} \approx 10\alpha_{\text{Sp}}$) and will hence give a much smaller contribution to the total dipole moment for phase-matching reasons (as long as the considered harmonic is part of the plateau). In turn, its contribution to the burden put on computing time is large since it introduces a rapid oscillation into eq.3.29.

Instead of considering a truncated Gaussian the incident laser beam shall for simplicity be approximated by a lowest-order Gaussian, which is sufficient for our qualitative consideration. The laser phase will then be

$$\phi_L = k_1 z - \arctan\left(\frac{z}{z_R}\right). \qquad (3.30)$$

In order to propagate the generated polarization, we need to solve the propagation equation [7]

$$\frac{\partial^2}{\partial z^2} E_q + k_q^2 E_q = -4\pi \left(\frac{q\omega_1}{c}\right)^2 P_q \qquad (3.31)$$

We take a Green's function approach [7, 9], that allows a very simple treatment. Equation 3.31 then has the solution

$$E_q(z') = \left(\frac{q\omega_1}{c}\right)^2 \int e^{ik_q Z} P_q(z) dz \qquad (3.32)$$

where $Z = z' - z$ denotes the propagation distance between the point of generation z and observation z'. $P_q(z)$ is proportional to $N_a(z) f_q(z, I)$ (cf. eq. 3.20), where $N_a(z)$ is again the atomic density.

This equation is fairly simple and allows an illustrative interpretation. $E_q(z')$ is the qth harmonic field, detected at point z', which consists of contributions from thin layers with width dz in the medium at position z. These contributions propagate to the detector at z', thereby acquiring and additional phase of $e^{ik_q Z}$.
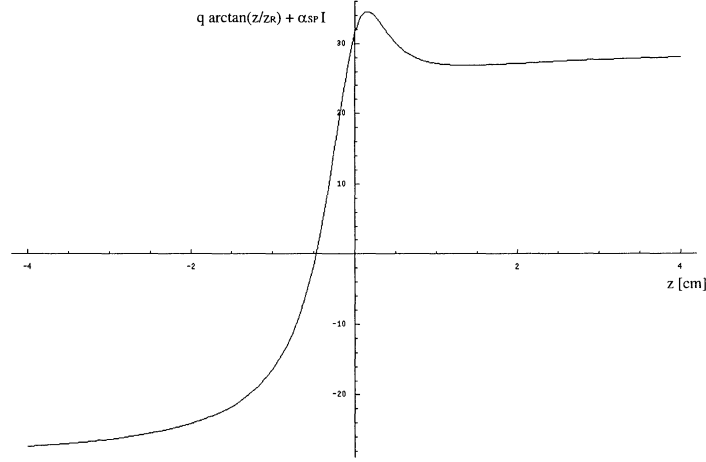
Figure 3.7: Phase difference $\Delta\phi$ between harmonic wave and polarization for the 19th harmonic, a pulse energy of 20 mJ and an iris diameter of 1.5 cm. The focus is at z=0, positive z are after the focus.

We finally take the constant $e^{ik_q z'}$ (hidden in the Z) out of the integral and forego writing z-independent, hence constant terms from now on. What we measure is of course an EMT current, which is proportional to the photon number per unit time $\Phi_q \propto |E_q(z')|^2$. We end up with

$$
\begin{aligned}
\Phi_q \quad &\propto \quad \left| \int e^{-ik_q z} P_q(z) dz \right|^2 \\
&= \quad \left| \int e^{-ik_q z} N_a(z) e^{iq(k_1 z - \arctan(z/z_R))} I^3 e^{-i\alpha_{SP} I(z)} dz \right|^2 \\
&= \quad \left| \int e^{i(-\Delta k z - q\arctan(z/z_R) - \alpha_{SP} I(z))} N_a(z) I^3 dz \right|^2 \qquad (3.33)
\end{aligned}
$$

Here, $\Delta k = k_q - qk_1$ is the wave vector mismatch between polarization and propagating harmonic field due to dispersion in the medium. This is usually -in the absence of free electrons- negligible compared to other contributions.
The total phase difference is

$$
\Delta\phi = \underbrace{k_q z}_{\phi_q} - \underbrace{(qk_1 z + \phi_{\text{dip}} - q\arctan(z/z_R))}_{\phi_q^{\text{Pol}}} \qquad (3.34)
$$

where the negative dipole phases of the short (and long) trajectory are represented by ϕ_{dip}.

Assuming dispersion to be small ($\Delta k \approx 0$) the phase variation across the laser focus looks like shown in fig. 3.7.
Phases are well matched when the curve in this plot is flat or even constant, since the wave vector mismatch, that shall be zero for perfect phase matching is

$$
\Delta k = \frac{\partial}{\partial z} \Delta\phi.
$$

This is achieved at z positions off the focus and best for $z > 1\,cm$, i.e. *after* the focus - so positioning the Ar medium represented by $N_a(z)$ here, should be a good idea. Of course there is an intensity $I(z)$ vs. phase matching tradeoff here and this consideration is just a small part of the whole picture.

Non-negligible multi-photon ionization gives another important contribution to the total phase mismatch since the presence of free electrons - whose density is strongly intensity dependent - changes the refractive index. This additional dispersion results in a wave vector mismatch as given in eq. 3.28

$$\Delta k_q^e = k_q^e - q k_1^e = \frac{\omega_p^2}{2cq\omega_0}(q^2 - 1)$$

hence we have to add a phase

$$\phi^e = \int\limits_{-\infty}^{z} -\Delta k_q^e(z')dz' \tag{3.35}$$

into eqs. 3.33, 3.34. Note, that the plasma frequency contains the electron density which varies rapidly across the focus - so this contribution plays a strong role in the intensity vs. phase matching tradeoff and seriously decreases the conversion efficiency for a medium position close to focus when the peak intensity is high enough to cause significant ionization.

Ionization

For our peak intensities this certainly was the case so we modelled ionization by roughly assuming an I^5 dependency of the ionization probability hence the electron density. The probability for the peak intensity was set to some $p_{i,max}$. Pulses as short as ours do not ionize the medium completely even at very high intensities. The correct treatment would be the Ammosov-Delone-Krainov theory that includes multi-photon ionization as well as optical field ionization.

Ionization then leads to a depleted medium, i.e. it cuts parts of the atomic density profile around the focus position. It further leads to a large dispersion due to the created free electrons. The brightness of the small blue plasma spark, that was visible in the gas medium when hitting it with the laser gave us an idea of when ionization was significant and when not.

Medium

The gas medium supplied by the jet-nozzle has been modelled with a Lorentzian with the experimentally estimated medium length as FWHM and cut at the wings, such that the total width was twice the estimated medium length. The shape of gas-jets as provided by simple jet-nozzles like our first one, has been examined by Altucci et al. [13] at a similar setup to the one we have used. They found a Lorentzian-like shape and a peak pressure of $\approx 40\,mbar$ at $0.75\,mm$ distance from the nozzle - corresponding to an atomic density of $\approx 9 \cdot 10^{17}\,cm^{-3}$.

Results

The integral (Eq.3.33, incl. the integral 3.35) has been solved numerically using *Mathematica*. The code can be found in Appendix A. The *Mathematica*-command `NIntegrate` uses an automatically chosen adaptive algorithm, which recursively subdivides the integration region as needed. It continues doing subdivisions until the error estimate it gets implies that the final result achieves the `PrecisionGoal` which is equal to the setting for `WorkingPrecision` minus 10 digits. A `WorkingPrecision` of n sets the precision used in internal computations to n digits. Though, even if internal computations are done to n digit precision, the final results may have much lower precision.

Medium position dependency

Since this model contains only the phase matching vs. intensity trade-off, we expect an advantage for the medium position after the focus.
We did this for 3 different iris-sizes for the 19$^{\text{th}}$ harmonic. The pulse energies corresponding to the iris size (we always cut the same beam, i.e. a smaller iris also reduces the pulse energy) have been determined experimentally to be $\approx 10\,mJ$ for an iris diameter of $w_i = 0.8\,mm$, $20\,mJ$ for a $1.5\,cm$ iris and $60\,mJ$ for a $2.5\,cm$ iris. They vary from day to day as the laser's condition varies but are reasonably stable within a range of $\pm 15\%$. The peak ionization probabilities were taken to be to 0.1, 0.2, 0.8, respectively.
Note, that the results shown in fig. 3.8 are plotted logarithmically.
  For the very small iris, the focusing is very loose and the intensities are not high enough to ionize the medium significantly - so the highest intensity in the focus pays off and we get a peak at that position. This changes for the larger irises. We obtain larger phase variations in the focus as well as stronger ionization. Clearly, phase matching favours medium positions off the laser focus. As already concluded from fig. 3.7, phase matching is better for the medium positioned after the focus. For the largest iris, the achieved intensity in the focus is maximal but still does not overcome the advantage of phase matching off the focus. Obviously we ran into some trouble with achieving the desired `PrecisionGoal` at z close to the beam waist leading to gaps in the plot and maybe values that should not be trusted. The rapid oscillation of the plot in this region proves the bad phase matching situation so we expect a dip there as well.
Note, that although the pulse energy in the last case is triple of that of the 1.5 cm iris and the beam is focused to a smaller spot, the reached photon number for the ideal medium positions are in the of the same order of magnitude. So we really do not benefit from the large energy.
The balance of the high intensity vs. bad phase matching trade-off near the focus depends strongly on β, which again is dependent on the harmonic order q and the kind of gas.
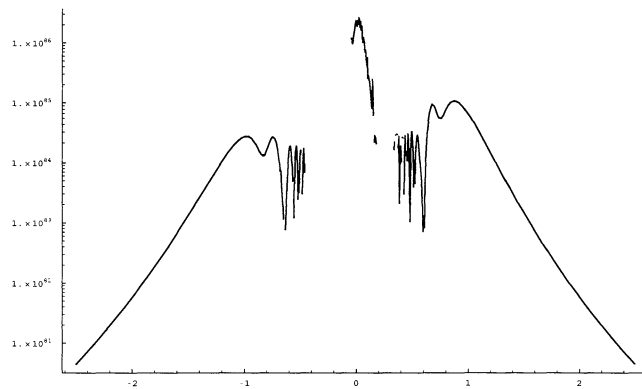In the experiment, we deal with a truncated Gaussian beam, whose intensity varies slower around the focus compared to a lowest order Gaussian, whereas th phase varies faster. Both will lead to some deviations from the results of this model.
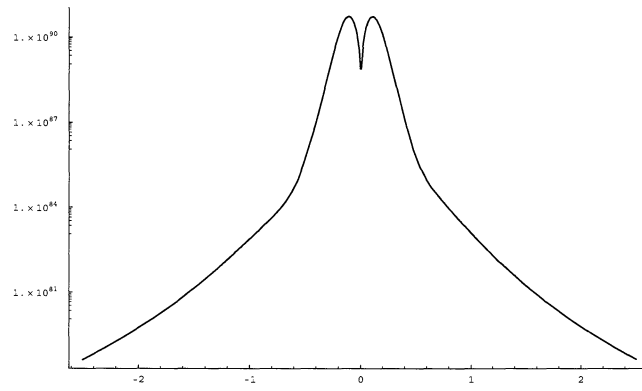
(a) Iris diameter of 0.8 cm (pulse energy = 10 mJ).
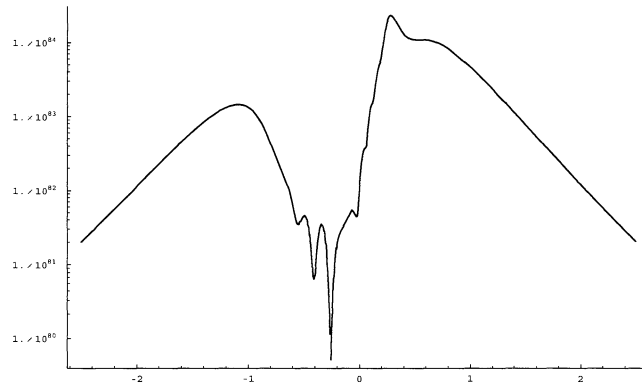
(b) Iris diameter of 1.5 cm (pulse energy = 20 mJ).

(c) Iris diameter of 2.5 cm (pulse energy = 60 mJ).

Figure 3.8: Medium position dependency of H19 for a 1.5 mm wide gas jet and different iris sizes as calculated with the 1D-model. The vertical axis shows the photon number in arbitrary units whereas the horizontal axis is the z axis of the model with values in cm. The focus is at z=0, positive z values are medium positions after the focus. (cf. fig. 3.9)

Missing Effects

As mentioned in section 3.1, free electrons due to multi-photon ionization and the induced refractive index change also produce the effect of a diverging lens. This leads to the preference of a medium position *before* the focus since here the converging beam might get collimated (self-guided) hence providing a larger effective interaction volume. This comes of course at the expense of a decreased peak intensity but we can very well afford this since we have a very large pulse energy. Placing the medium right after the focus allows to obtain the maximal intensity with good phase matching but leads to an increase of the divergence in presence of ionization hence a smaller interaction volume with sufficiently high intensity to effectively generate harmonics (cf. fig. 3.9). Still high order harmonics that rely on the availability of the highest possible intensity will only be generated with this medium position. (Lower order) plateau-harmonics should -provided that ionization and hence the effect of self-defocusing is large enough- be more efficiently generated *before* the focus as for them it is not tragic if the intensity decreases by a certain amount and they will benefit from an increased generation volume.

It is hard to model this effect with some simple addition to the existing framework and doing a proper simulation by solving propagation equations for ionizing media is beyond the scope of this qualitative model. This was done by H.T. Kim et al. [10], whose work was mentioned in section 3.1 before.

Whether the medium position before or after the focus gives the best result depends on the impact of both the effects of phase matching and self-defocusing and is not predictable with the rough assumptions made in our model. Often [10, 11, 12], the medium position before the focus was found to give the best
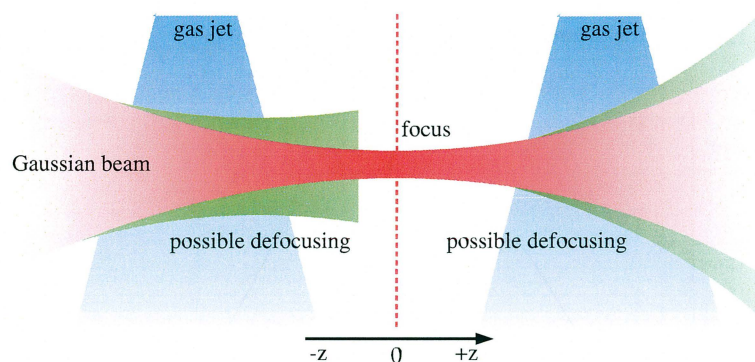

Figure 3.9: Possible medium positions in the beam and the self-defocusing effect. If the medium is placed before the focus of the Gaussian beam, the focus becomes larger and shifts, but the beam might get well collimated. In the medium after the focus, the divergence becomes larger but the achievable peak intensity at the medium entrance is larger.

harmonic generation efficiency - but only for lower order harmonics that do not rely on the maximum available intensities.

For ultra-short pulses and a loose focusing geometry the impact of phase-matching and self-focusing will certainly decrease and one possibly cannot neglect re-absorption any more. This has been studied by Eric Constant et al. [14], who conclude that it is re-absorption that sets the limit to a maximum useful medium length.

Chapter 4

Optimization

In this chapter experimental data will be presented and interpreted in terms of our model of HHG.

Long scans of all observable harmonics and the highest observable orders will be presented in a first section, allowing to get an overview of the spectrum being dealt with. Then we will discuss the influence of some parameters on the harmonic generation efficiency.

4.1   Experimental Conditions

We first describe all in detail all of the experimental parameters.

Entrance and Exit Slits

The entrance slit is situated before the spectrometer, cutting a significant part of the harmonics as well as the noise. It is generally assumed that the actual harmonic intensity is linearly dependent on the slit opening, if the slit is aligned to be approximately in the center of the generated beam, which was verified during the alignment.

Many measurements were carried out with a 100 μm slit opening, which was great for noise reduction, but if higher signal strengths were required, it could well be opened up to 250 μm or even 500 μm in some cases. Measurements whose absolute intensity is to be compared will always have the same entrance slit size.

The exit slit is mounted after the spectrometer and before the EMT. It was constant at 100 μm and was not changed in any of the experiments.

EMT Voltage

The Electron Multiplier Tube's normal voltage of operation was 4000 V, only in the beginning some measurements were conducted with 3500 V, but this led to a weaker signal and thus was corrected for all data presented in this chapter. A calibration of the EMT signal in photon number was not conducted in our studies. This is one of the reasons, why all spectra only show arbitrary units for the photon number. This may make the comparison between the different experiments more difficult, but since the EMT signal was dependent on many

parameters and especially the alignment, the calibration conducted at one point would for sure have been invalid again at another.

If such a comparison is made in any figure it is assumed that the alignment and EMT conditions will have changed only slightly between two scans directly following one another. The scans were conducted in ascending or descending order, allowing to usually compare a point with its surrounding points.

Spectrometer

After alignment of the spectrometer that made the steering unit's number correspond to the grating position, the wavelength region from the 11th harmonic was the lowest that could be observed, approximately at a grating position of 168. But seldom we extended our scans down to this region, since our main interest lay on the higher harmonics around the 19th order and beyond. The 31st or 33rd order were the highest that were still observable, mostly because the signal-to-noise ratio was too bad to resolve any more harmonics. Also, the step size of the motor that turned the grating does not allow to distinguish the harmonics any more at these high orders, even though the intensity would be high enough to see even higher orders. This was not the aim of our experiments, but the resolution could have been improved by the introduction of the Jobin Yvon's other grating for lower wavelengths.

Applying the theoretical cut-off law with Argon's ionization potential of $15.8\,eV$, a Ti:sapphire laser with 800 nm wavelength and an intensity of $5 \cdot 10^{14}\,W/cm^2$ gives a cut-off position around the 41st order. Although this prediction cannot be expected to be reached experimentally, we should have been able to reach up to a few orders higher with some optimization. It is typical for Argon to exhibit a first plateau followed by another, lower one until the real cut-off is finally reached. This lower one is what we could not resolve anymore.

Pulse Energy

The energy per pulse actually being focused into the medium (neglecting losses in lens, propagation and entrance window) is of course dependent on the iris aperture before the entrance window to the vacuum chamber. The standard conditions for our setup were mainly $260\,mJ$ per pulse before the compression of the pulse.

The energy after compression can be seen from figure 4.1 which reflects the intensity profile of a Gaussian beam fair enough. This also shows that for an aperture of $1.5\,cm$ - the one we used for most measurements - the pulse energy is slightly above $20\,mJ$.

It is important to note that the beam after the iris will no longer be of Gaussian profile but rather of that of a truncated Gaussian. This one of the reasons for our rather loose focusing, that has relatively little intensity variation over a great area around the focus. One advantage of this is the great manoeuvrability of the medium over the focus without losing the necessary intensities for the harmonic generation process.
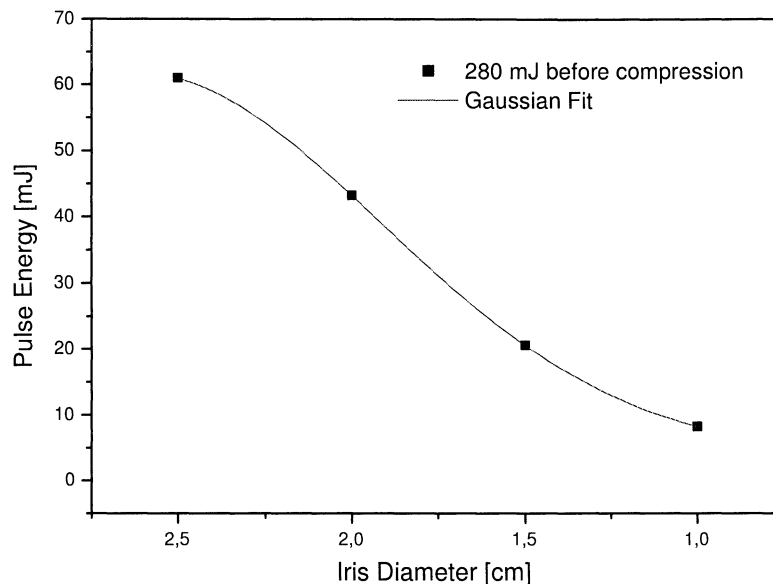
Figure 4.1: Pulse energy after compression, depending on entrance aperture size.

4.2 General Spectra

Quite many longer scans were performed, mostly for purposes of getting an overview and to compare the experimental conditions between different measurements. A selection is shown here, also to compare the results of the different nozzles used. The intensity of these studies can hardly be compared with each other, since most of them were just snapshots at momentary conditions, only roughly defined in their parameters. They do, however, give a general idea.

Measurements and Conclusions

Figure 4.2 shows two spectra that were obtained at different medium positions in relation to the focus of the laser beam. In Figure 4.3(b) a long scan obtained with the fat tube nozzle (2.5 mm) can be seen. The medium was situated quite far from the focus, approximately 3 cm. Finally, Figure 4.3(a) shows the harmonic spectrum with the medium position 2.5 cm from the focus using the newly built thin tube nozzle of 1 mm diameter. One important observation is that the highest orders are more easily observed if the medium is situated close to the focus. Still it has to be taken into account that good phase matching is more difficult to achieve at these positions.
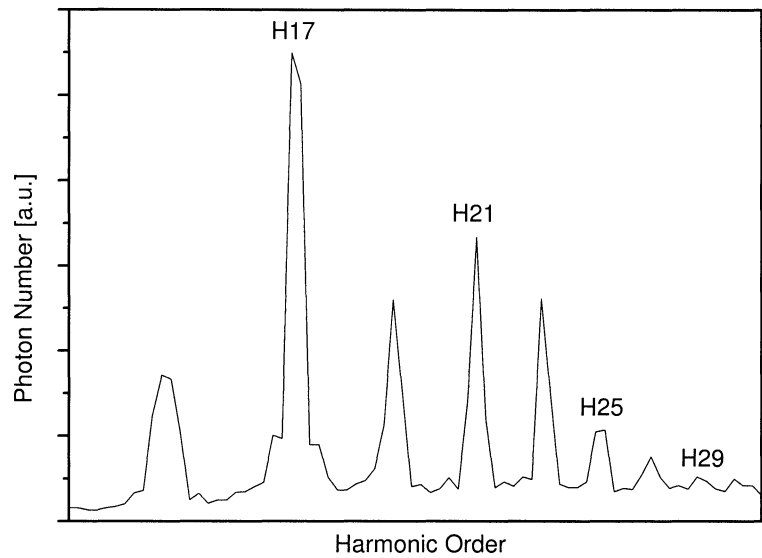
(a) Spectrum with medium 3.5 cm after the focus. It is obvious that higher orders are more difficult to observe, if the medium is situated further away from the focus.
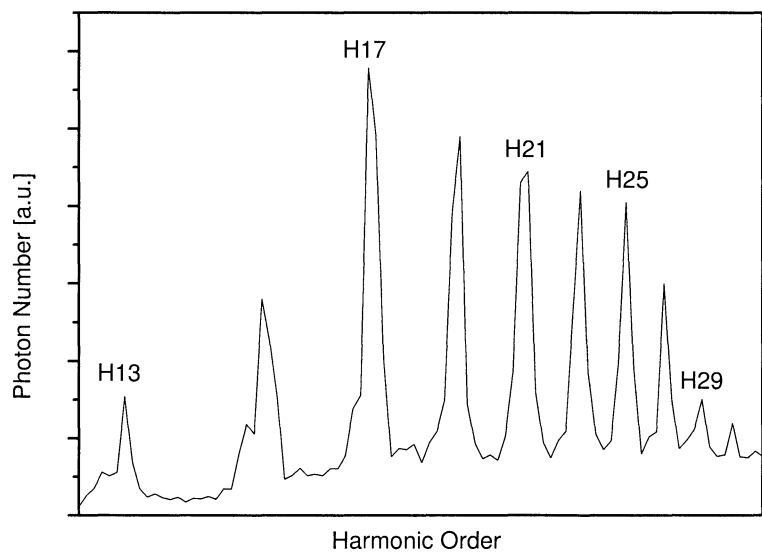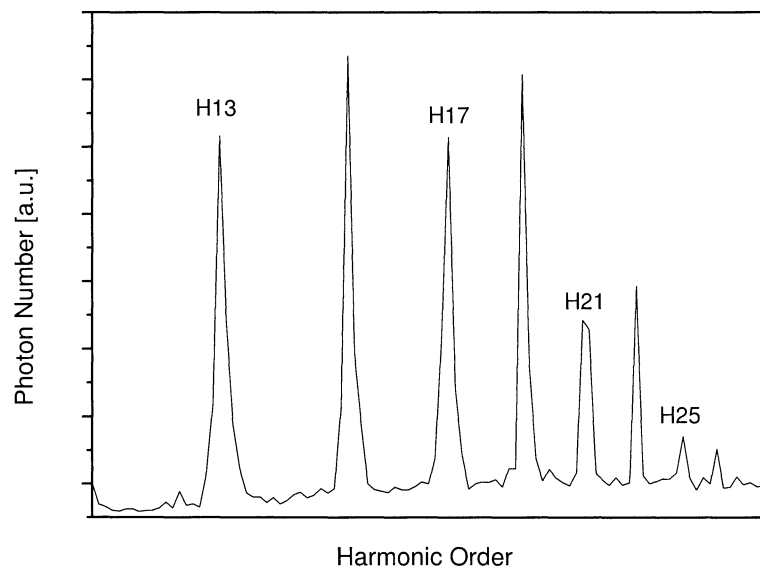

(b) Spectrum with medium 1 cm after the focus. The 31st harmonic is very clearly visible, before further harmonics will vanish due to the small resolution of the spectrometer.

Figure 4.2: Harmonic spectra of Argon at different medium positions.
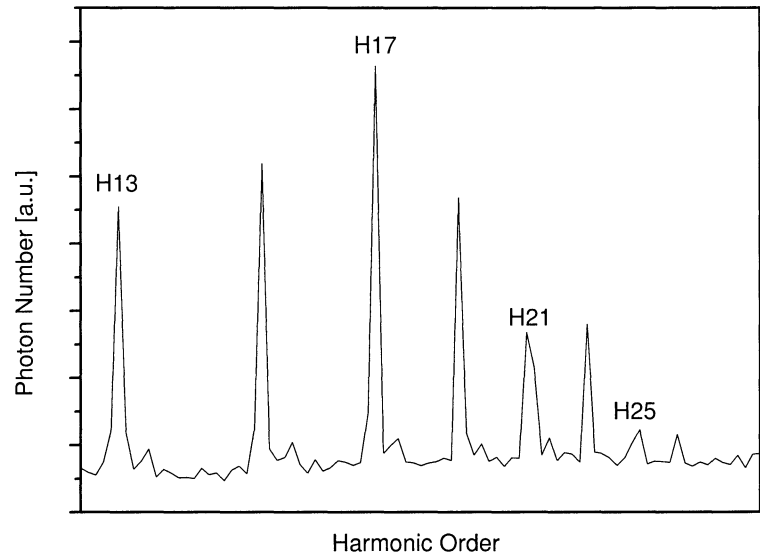
(a) Harmonic spectrum of Argon, obtained with thin tube nozzle and the gas medium 2.5 cm from the focus

(b) Harmonic spectrum of Argon, obtained with fat tube nozzle and the gas medium 3 cm from the focus

Figure 4.3: Harmonic spectrum of Argon, generated with either of the tube nozzles.

Double Peaks

When measuring the harmonic spectra quite often we encountered double peaks as seen in figure 4.4 for the 19$^{\text{th}}$ harmonic. In the harmonic peaks, small red and blue satellites may occur symetrically around the main large harmonic peak due to the contribution of the second trajectory, as has been shown in [15]. But since the satellite was quite often observed as red, it would not easily reveal its secret. That is why more thorough studies of the double-peaks' origins were conducted with the fat tube nozzle.

The generated harmonics have a spatial chirp, a radial frequency variation over the beam profile [15]. Since our entrance slit of the spectrometer allows to choose from several slit widths, each slit separated from another by a plate, one of these plates might block a part of the frequency spectrum inside one harmonic beam profile, while having two different parts of the harmonic pass through two different slits. This would then lead to a breach inside the otherwise continuous spectrum of the harmonic peak. The whole concept of this is sketched in figure 4.5. Figure 4.4 is one of the spectra taken to study the parameters responsible for the double-peaks. When the entrance slit was opened up very wide (which was possible in the vertical dimension), the structure was transformed to a very broad harmonic peak and when the slit was shifted horizontally perpendicular to the beam axis, one peak vanished in the structure. This data led to our assumption of the spatial chirp, regarding the double peaks as related to alignment and experimental setup and thus not as real physical effect occuring in the experiment. This is of course just one possible explanation, many questions still remain to be answered. To be able to make a more precise statement, further studies would be necessary. For example the question of the medium position would have to be solved as the double peaks were more likely to occur with positions before the focus. Also, the spatial distribution of the chirp is not necessarily perfectly symmetric and dependent on the harmonic order.

4.3 Pressure

Clearly, the backing pressure of the gas valve has an influence on the medium, the atomic density determines many parameters such as electron density or the refractive index itself. Thus studies of the pressure dependence of signal and spectral characteristics will be presented in this section.

Measurements and Conclusion

In figure 4.6(a) there appears to be a dip at 1200 *mBar* of pressure, which we assume to be an artefact for example due to a decrease in laser intensity), since we were not able to reproduce this result in other series. In general, one can see from the figures that the pressure increases the harmonic gain only up to a certain level, and from about 1000 *mBar* on it appears to start saturating. Especially with the fat tube nozzle an interesting effect occurs, when the intensity appears to decrease again in the end. Even though these results should not be trusted too much due to the rather large errors involved in all these measurements, it might seem reasonable that increased atomic density could lead to increased reabsorption.
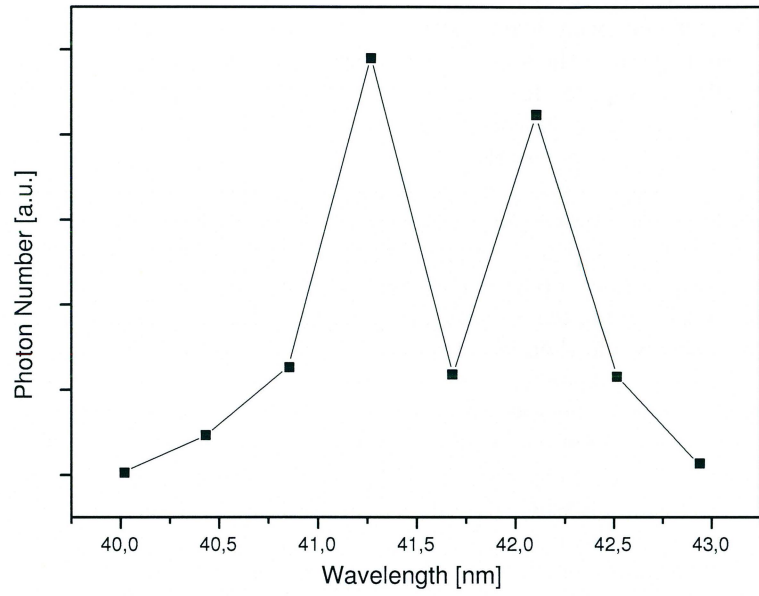
Figure 4.4: 19th harmonic with characteristic double-peak structure
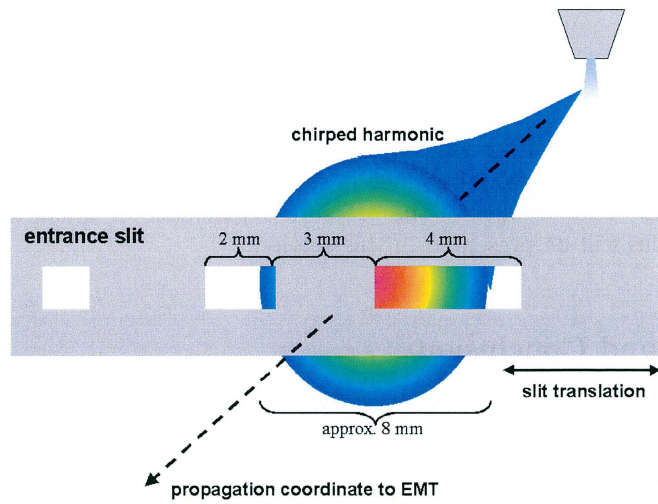

Figure 4.5: Schematic of how the spatially chirped harmonic with the spectrometer's entrance slit leads to a double-peak structure.

So the reason why the atomic density should not be increased infinitely is that at the same intensity with a larger number of atoms the ionization probability is of course the same and thus the electron density is increased, leading to an increased phase mismatch in the harmonic generation process. With the high intensities maintained over long distances in our focused truncated beam, this is even more important for the long media of the tube nozzles.

4.4 Medium Position

The position of the medium in relation to the laser beam focus is of importance in several terms. If the medium is placed right in the focus, the intensities available for the process are the highest but since many unwanted processes' likelihood also scales with the intensity an actual gain may seem questionable. In addition, phase matching is more difficult in the focus due to the faster phase variation of the incoming beam. On the other hand the placement of the medium too far from the focus may reduce the intensity below that required for significant harmonic emission.

Measurements

The dependency of the harmonic peak intensity on the position of the medium in relation to the focus is shown in figure 4.7 for different harmonics. Figure 4.8 shows the lens position for different nozzles. The problem with the thin tube nozzle was in this case that it could not be moved to the other side of the focus, since there the laser beam hit the nozzle itself and would have possibly harmed it. Figure 4.7(a) together with figure 4.9 shows the dependency of the harmonic signal on the iris aperture and thus the pulse energy.

Conclusions

The results in figure 4.7 seem rather unexpected, since they could not be reproduced in our model. The common shape of all graphs is that of a bad situation in the focus due to reasons of phase matching and higher ionization. But where the other figures have the preferred medium position behind the focus, its best position here is that in front of the focus. A possible explanation, which has not been included in the model, might be the effect of self-defocusing, as was illustrated in figure 3.9 in chapter 3.4. This would lead to a collimated beam, and can greatly improve phase matching as has been shown [10].
All the other plots mainly support the interpretation of the model presented above that by terms of phase the position after the focus is favoured over that before the focus. Figure 3.7 shows the different phase matching situations over the focus and its impact is already being dealt with in section 3.4. As mentioned, the high intensities in the focus also increase ionization processes.
Compared to our model, the positions with best generation efficiency are further away from the focus than predicted, which we attribute to the fact, that we assumed a lowest order Gaussian beam but are in fact dealing with a truncated Gaussian. The intensity varies slower in this case so our z axis gets "stretched".
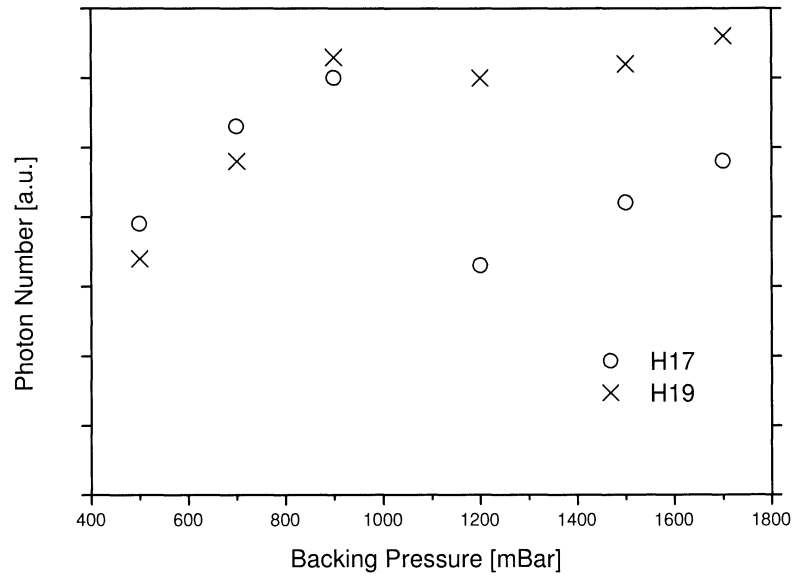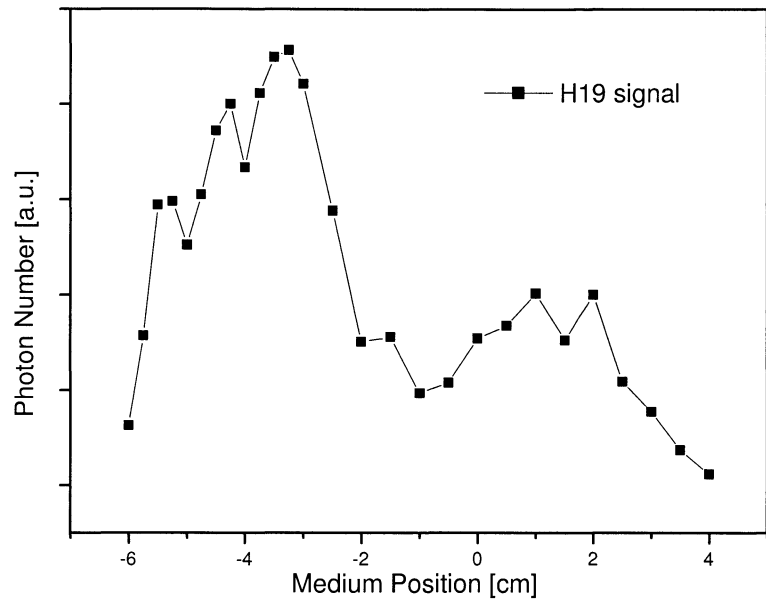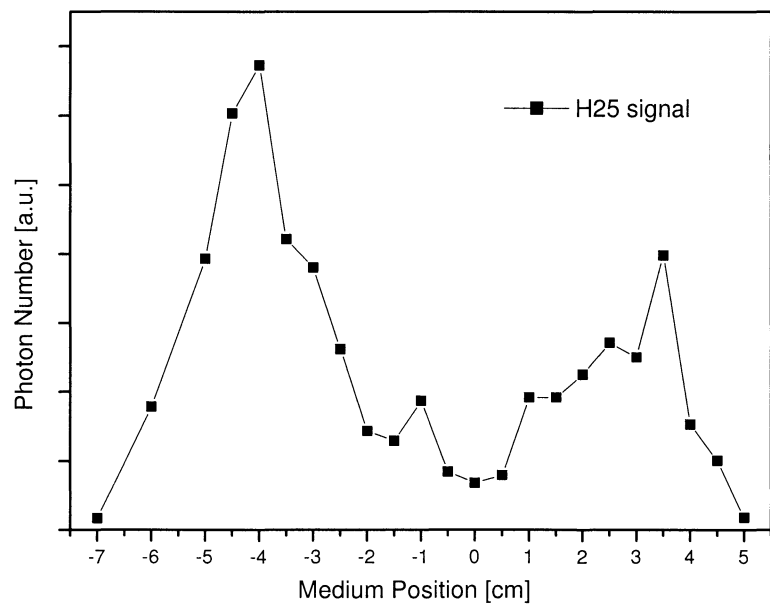
(a) Thin tube nozzle
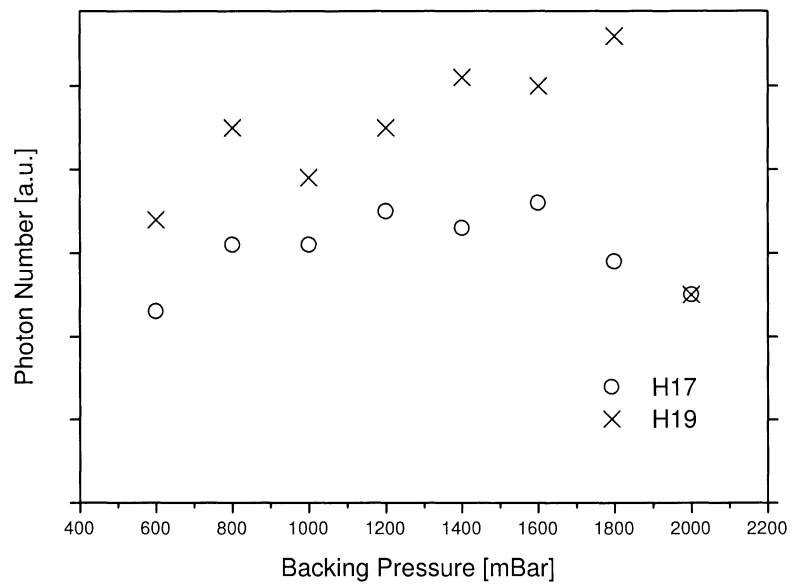
(b) Fat tube nozzle

Figure 4.6: Pressure dependency of the peak intensity of 17th and 19th harmonic with the two tube nozzles.
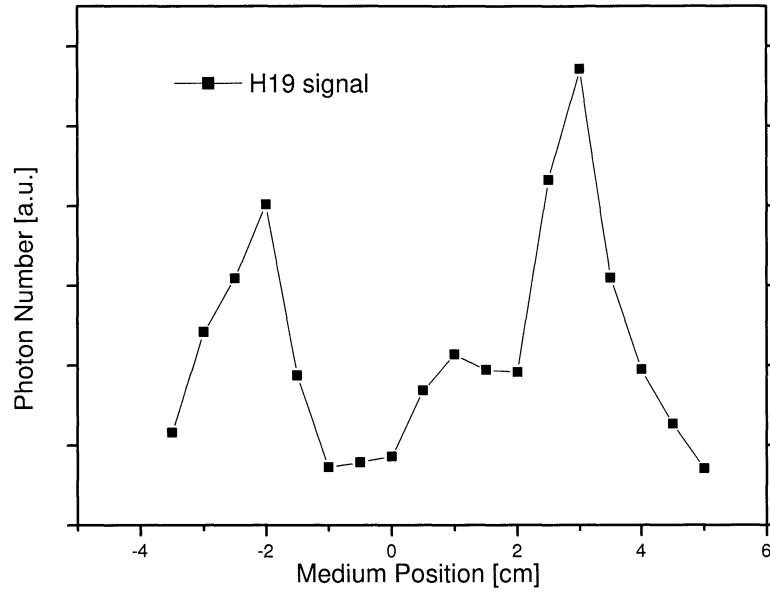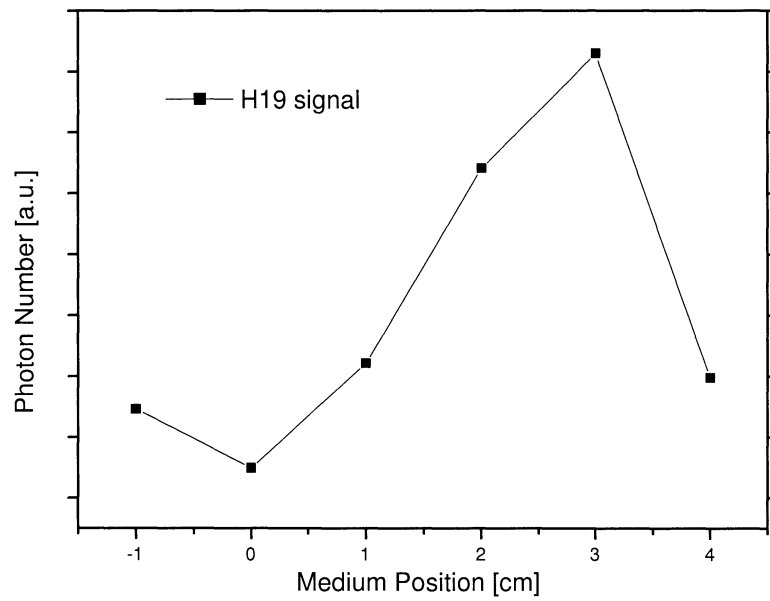
(a) 19th harmonic

(b) 25th harmonic

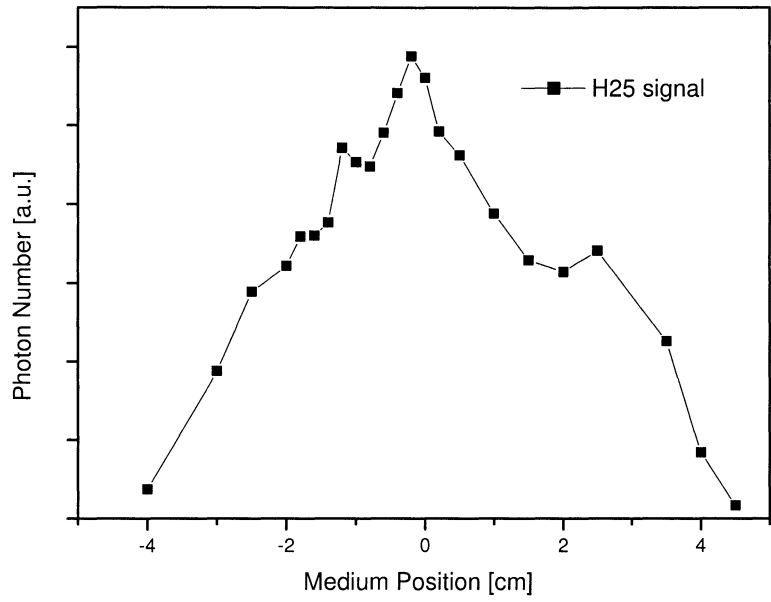Figure 4.7: 19th and 25th harmonic with 1.7 cm aperture and jet nozzle.
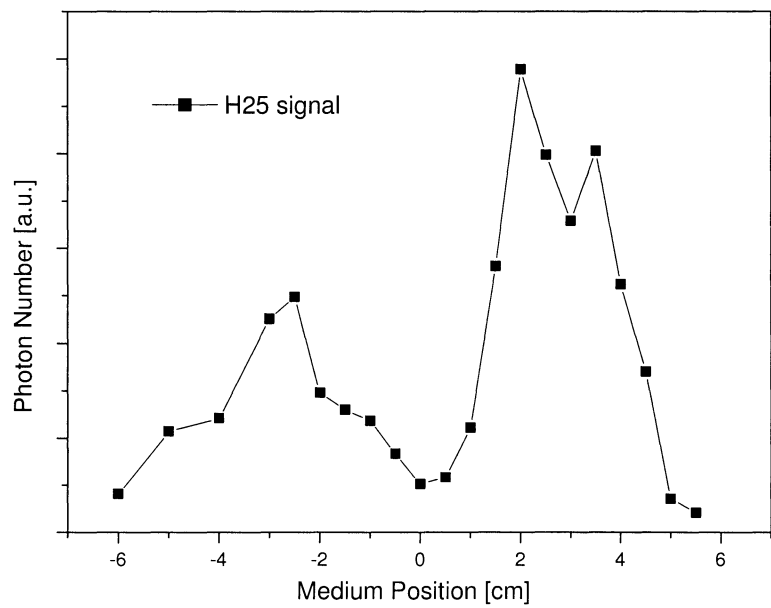
(a) fat tube nozzle.

(b) thin tube nozzle

Figure 4.8: 19th harmonic with 1.5 cm aperture and different nozzles.

(a) 25th harmonic with an aperture of 0.8 cm

(b) 25th harmonic with an aperture of 2.5 cm

Figure 4.9: 25th harmonic with different apertures and jet nozzle.

4.5 Aperture

A study of the intensity of the 19th harmonic depending on the entrance aperture and thus also the pulse energy was conducted with the fat tube nozzle. Of course the aperture influences the harmonic generation in several ways. The spot size at the focusing lens has an influence on the spot size in the focus, and thus the intensity distribution. This also influences the phase variation over the focus, so that many parameters are varied at once with the entrance iris aperture.

Measurement and Conclusions

Figure 4.10(a) shows a scan over aperture widths resulting in a two-peak-shape, where the one for smaller irises is higher. A possible explanation for that is found from the argument that with a smaller aperture the focus will in general be larger, the phase will vary slower and and allow phase matching to be achieved more easily. On the contrary, with larger apertures the sheer force of high intensity and large amounts of energy begin to dominate over the losses of the increasingly difficult phase matching process. The transition between both regimes is marked by the dip between the two peaks. The same two peaks can be seen in figure 4.10(b) where the same scan has been done for the jet nozzle. There it is interesting to see that the second peak is of same height, which is not the case with the tube nozzle.
A dependency like this has been studied by Kazamias et al. [16] who observed the aperture dependency with a setup very similar to ours -except for beam size and energy- of H21 in Argon. They found a clear peak for the generation efficiency followed by a rapid decrease showing some oscillation.
It is apparently more useful to favour phase matching over the highest intensity in the focus, as seen for the tube nozzle. The much greater medium length allows greater gain for good phase matching conditions, which are harder to achieve for a large aperture. With the jet nozzle it is apparently of greater importance to make the best use possible of the available medium, which is not a very large volume with a length of approximately 2 mm.
In conclusion, for our beam properties the improvement of phase matching seems to be more important to optimization of harmonic generation than intensity alone.

4.6 Nozzles

As seen already, we used three different types of gas nozzles in our experiment to shape different media for the HHG process. The jet nozzle with the simple gas jet, the thin tube nozzle and fat tube nozzle, each of which yields four to five times the medium length of the jet nozzle. For greater detail refer to section 2.2.
If we are actually improving the generation efficiency with using a longer medium is not clear yet since the data for the jet nozzle were taken weeks before the introduction of the tube nozzles to the setup so they are hard to compare. Though, based on the apparently very good phase matching conditions (cf.fig.
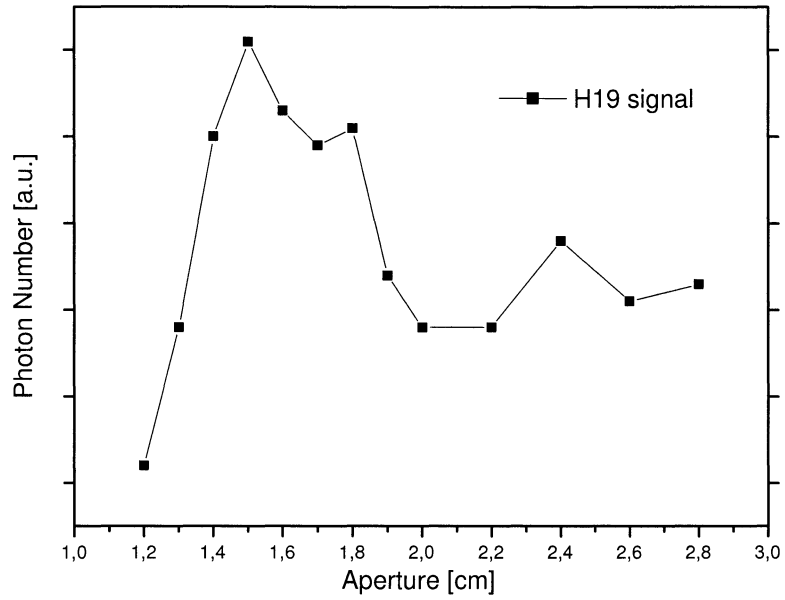
(a) 19th harmonic with fat tube nozzle.
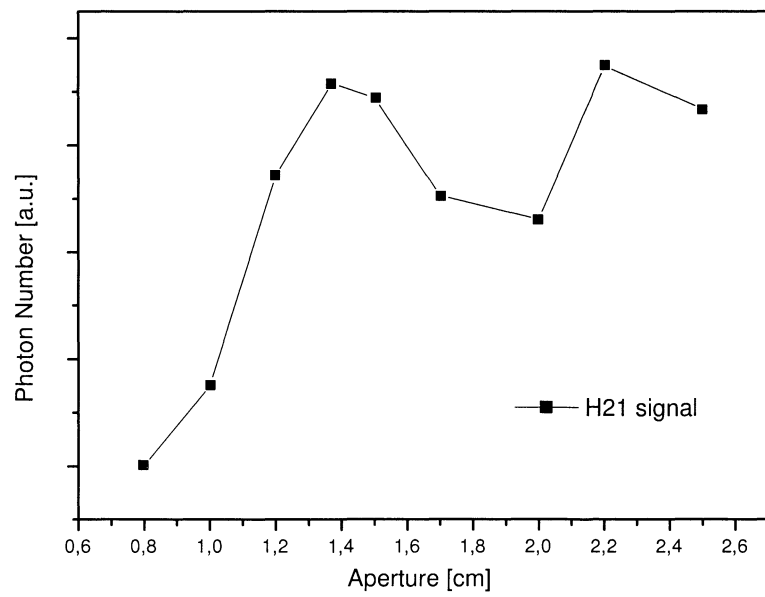
(b) 21st harmonic with jet nozzle.

Figure 4.10: Harmonic signal dependent on aperture size.

3.7) and the fairly slow variation of intensity after the focus we really expect this approach to lead to an improvement.

Conclusions

At quite an early stage we assumed that the medium length of the jet nozzle could be improved by construction of a more complicated type. Also the pressure distribution inside the nozzle is assumed to be more homogeneous inside the tubes, resulting in a more symmetrical setup in the propagation direction, which might prove useful for phase matching. A gradient in atomic density perpendicular to the actual beam propagation might complicate the matching that is necessary with the geometrical phase. The thin tube nozzle quite surely is narrow enough to allow the assumption of symmetry in its gas pressure distribution. The fat tube nozzle might not allow this assumption yet, since there is quite a great flux of gas due to the constant pumping. Therefore this nozzle might be furtherly improved by closing the ends of the nozzle with some material and creating a pinhole by the focused laser beam. In general, symmetrical and homogeneous media appear to be favourable.

Chapter 5

Application

5.1 Characterization of ultra-fast VUV sensitive photo-diodes

In a campaign together with Prof. Jörgen Larsson from LTH as well as Prof. Eugene Kennedy and Dr. John T. Costello from the "National Centre for Plasma Science & Technology" at the Dublin City University we tried to detect harmonics with very fast photo-diodes. Mostly Schottky diodes are used for VUV detection and there are also GaAsP diodes - but both have a very slow response time of microseconds. The idea for their application is to precisely measure the delay between two laser pulses - one of them in the IR and the other one in the VUV spectral region.

In particular we had the Free Electron Laser at DESY in Hamburg in mind that currently is under construction where these diodes would offer a very cheap possibility to supply each user with an own delay control. The VUV pulse would be produced by the FEL whereas the IR pulse would be coupled out of the seeding laser and hence would be naturally synchronized to the FEL output. This IR pulse could be amplified again in an amplifier stage and be used for pump-probe measurements where a precise delay control is desired. For this purpose we need to have a time resolution of better than say $100\,ps$ (or $3\,cm$ of optical delay) so that we could get the FEL and IR laser pulses very close in time before adjusting the time delay using micrometer controlled translation stages. Obviously we also need the diode to be both IR and VUV sensitive and have a rise time of $< 50\,ps$. To measure rise times of this order with VUV light we need very short pulses - a requirement that is best fulfilled by high harmonics of an ultrashort laser.

The diodes under examination were fast commercial PIN GaAs diodes (ET2000) for applications in communication techniques with a rise time of $< 40\,ps$ that are designed for IR light that is coupled onto them from a fiber. We drilled out the coupling lens to expose the PIN diode directly. Though, if the diodes were sensitive to VUV light at all was not sure. To reach the desired speed, their capacitance had to be reduced hence they had to have a very small active area of approx. $40\,\mu m$ x $40\,\mu m$. To detect our harmonics, the biggest problem was to discriminate against the many orders of magnitude stronger IR background of the fundamental. In order to do so we could simply replace our EMT with

46

a diode, which has the advantage of having split off the fundamental beam. However, we also fan out the harmonic beam with the grating hence reduce the number of photons that hit the diode. In addition, approx. only one of a hundred photons makes its way through the spectrometer which reduces the photon flux further. The estimate of the necessary rate of harmonic photons that had to hit the active area of the diode to obtain a measurable signal voltage was a few thousand photons per second. If we assume a rate of generated photons per harmonic of 10^8 and take the spectrometer's efficiency as well the ratio of the diode's active area ($\sim 10^{-9}\,m^2$) and the area of the harmonic beam ($\sim 10^{-6}\,m^2$) into account we find that we might just reach this limit. We had to remove the spectrometer's exit slit since the beam going trough it was directed upwards and we were not able to align the diode in such a way that the beam hits its active area. Removing the exit slit made that possible but also let a huge amount of IR light scattered by the shiny inside of the spectrometer into the chamber containing the diode, which made an aluminium filter right in front of the diode necessary, that absorbs IR light but transmits ($\approx 60\,\%$) the VUV. Unfortunately after a careful alignment and an extensive scan of grating and diode positions we did not see any VUV signal. That could have either been due to the too small number of harmonic photons reaching the diode or of course because the diode just was not sensitive to the wavelengths that it was exposed to. We mainly tried to direct the 17$^{\text{th}}$ or 19$^{\text{th}}$ harmonic onto the diode since these were the ones we had optimized before.

Another possibility was to remove the spectrometer and benefit from the fact that the divergence of the fundamental beam is larger than the one of the harmonic beam hence at a distance of approx. 1.50 m after the harmonic generation chamber, the fundamental beam intensity will have significantly decreased. So with a few irises in the beam line after the generation chamber that cut away large part of the fundamental and only let the harmonic beam pass, combined with an aluminium filter we should be able to direct the complete harmonic beam (i.e. containing all orders that are transmitted by the aluminium filter) onto the diode and keep the IR background down to a level that allows to detect the expected very weak VUV signal. This should give a much larger harmonic photon flux onto the diode than the first approach, but again we did not have success.

The conclusion would be that the harmonics either were too weak - but before attaching the diodes we checked the harmonics with our usual setup and found them to be reasonably strong. Also, at least in the second approach the alignment was a lot easier and more or less all generated harmonic photons should have made their way to the diode - so we exclude this explanation for the failure. It remains another possibility - namely that the diodes simply were not sensitive to VUV radiation at all.

To answer this question, the manufacturers of the diodes will be asked for details on the construction - a thin (even 50 nm) oxide layer will greatly attenuate the VUV. It will also be checked for their sensitivity in the UV with the 3$^{\text{rd}}$ harmonic of an 800 nm Ti:sapphire laser at MAX-lab in Lund to go in smaller steps from the IR, for which the diodes are actually designed, toward shorter wavelengths. Still, to measure a rise time of the order of ps with VUV radiation, there is no other way but to use high harmonics.

Chapter 6

Conclusion

During this project we succeeded in the construction and operation of a beam line for measuring high-order harmonics. Since much of the setup had been dismantled and torn apart, quite some effort was spent before its actual reactivation had taken place. We described the setup in detail and introduced several slight improvements such as providing the best vacuum at the EMT, where it is most needed and allowing the maximum pressure in the whole system to be estimated by the position of the pressure meters. By the construction of a novel type of gas nozzle, the setup was also furtherly extended.

The theory of high-harmonic generation was used for a one-dimensional model, that allowed to reproduce quite a large number of experimental results and can be applied and extended in the future. To continue in this field, self-defocusing could be included. Also the assumptions for some parameters involved could be more justified.

The optimization of the harmonic generation proved to be quite difficult in our case, since it is a multiple parameter problem, and due to changing conditions it is relatively difficult to compare the results from one day to another. The introduction of the new nozzles led to a different problem, when it appeared that the setup was mainly designed for radially symmetric nozzles. Thus certain sacrifices in the pumping pressure were made, which also might have affected the EMT signal. In conclusion, our data allows more of a qualitative interpretation and lacks comparability. More systematic and continued studies are required in the future.

An application for the ultraviolet pulses has been presented and studied, but the VUV-sensitivity of the diode could not be validated. This field of study is also to be continued.

Acknowledgements

Bibliography

[1] L. Roos, Optimisation and Application of Intense High-Order Harmonic Pulses, PhD Thesis, Lund Institute of Technology, **LRAP-276**, 2001

[2] J. Mauritsson, Temporal Aspects of High-Intensity Laser-Matter Interactions, PhD Thesis, Lund Institute of Technology, **LRAP-312**, 2003

[3] S. Svanberg, J. Larsson, A. Persson and C.G. Wahlström, Lund high-power laser facility - systems and first results, Phys. Scr. **49** 187, 1994

[4] R. Boyd, Nonlinear Optics, 2nd Edition, Academic Press, 2003

[5] O. Svelto, Principles of Lasers, 4th Edition, Plenum Press, 1998

[6] M. Lewenstein and A. L'Huillier, Principles of single atom physics: High-order harmonic generation, Above-threshold ionisation and non-sequential ionisation, Springer, 2002

[7] A. L'Huillier et al., High-Order Harmonic Generation In Rare Gases, Atoms In Intense Laser Fields, Academic Press, 1992

[8] P. Johnsson, *private communication*, 2004

[9] V.T. Platonenko et al., Control of the angular structure of high-order harmonics, Quantum Electronics, **34**(1) 71-75, 2004
Vitali Strelkov, *private communication*, 2004

[10] H.T. Kim et al., Optimization of high-order harmonic brightness in the space and time domains, Phys. Rev. A **69** 031805(R), 2004

[11] H. Sakai and K. Miyazaki, Effect of multiphoton ionization on high-order harmonic generation and propagation in rare gases with subpicosecond laser pulses, Phys. Rev. A, **50**(5) 4204, 1994

[12] K. Miyazaki and H. Takada, High-order harmonic generation in the tunneling regime, Phys. Rev. A, **52**(4) 3007, 1995

[13] Altucci et al., Influence of atomic density in high-order harmonic generation, J. Opt. Soc. Am. B, **13**(1) 148, 1996

[14] E. Constant et al., Optimizing High Harmonic Generation in Absorbing Gases: Model and Experiment, Phys. Rev. Let., **82**(8) 1668, 1999

[15] M.B. Gaarde, F. Salin, E. Constant, Ph. Balcou, K.J. Schafer, K.C. Kulander and A. L'Huillier, Spatiotemporal separation of high harmonic radiation into two quantum path components, Phys. Rev. A, **59**(2) 1367, 1999

[16] S. Kazamias et al., High order harmonic generation optimization with an apertured laser beam, Eur. Phys. J. D, **21** 353, (2002)

Appendix A

The Mathematica Code

```
(*for 1.5cm iris, 20mJ pulses, peak ionization probability=0.2*)
(*everything in cm*)

(*pulse mean power*)
P=0.02/10/(35*10^-15)

(*wavelength*)
lambda=800*10^-7

(*focal length*)
f=100

(*iris radius*)
wi=0.75

(*harmonic order*)
q=19

(*amplitude of dipole moment*)
aq=i^3

(*dipole phase proportionality constant, short path*)
asp=2*10^-14

(*beam waist radius*)
w0 = (lambda*f)/(pi*wi)

(*rayleigh length*)
zR = pi*w0^2/lambda

(*gaussian intensity z-profile*)
I = P/(pi*w0^2*(1 + (z/zR)^2))

(*gouy phase shift*)
phig=ArcTan[z/zR]
```

```
(*medium length*)
w=0.15

(*normalized atomic density profile, centered around z0*)
n= 1/(4((z-z0)/w)^2+1)* (1-UnitStep[z-z0-w])*UnitStep[z-z0+w]

(*ionization probability*)
Pi = 0.2*(I/(P/(pi*w0^2)))^5

(*density of ionized atoms = created electron density*)
Dn=Pi*n*9*10^17*10^6

(*wavevector mismatch due to free electrons - this time everything in m,
then *10^-2 to get cm^-1*)
Dke=(q^2-1)*Dn*(1.602*10^-19)^2*lambda*10^-2 /
(9.109*10^-31*8.854*10^-12*4*pi*299792458^2*q) *10^-2

(*the same, but z renamed x*)
Dkex = 50714.95436206033'*(-1 + q^2)*lambda*(1 - UnitStep[-w + x - z0])
*UnitStep[w + x - z0]  /  (q(1 + (4*(x - z0)^2/w^2))
(1 + (pi^2* wi^4* x^2)/(f^4*lambda^2))^5)

(*phase mismatch due to free electrons, integration of Dke from a point
 where the electron density is zero to z*)
Dphie:=  NIntegrate[Dkex ,{x,-3,z}, WorkingPrecision -> 50]

(*integrand for the next step*)
Nd:=(1-Pi)*n *  Exp[i(-q*phig-Dphie)]*(aq* Exp[-i*asp*I])

(*number of harmonic photons at order q*)
S:=(Abs[NIntegrate[Nd  ,{z,-3,3}, WorkingPrecision -> 50]])^2

(*Plot the photon number vs. the medium center-position*)
Plot[S, {z0,-2.5,2.5}, PlotRange ->  All]

and here comes the plot...
```